Contrast Pattern Mining in Paired Multivariate Time Series of Controlled Driving Behavior Experiment

QINGZHE LI, George Mason University, USA

LIANG ZHAO, George Mason University, USA

YI-CHING LEE, George Mason University, USA

JESSICA LIN, George Mason University, USA

Controlled experiment is an important scientific method for researchers seeking to determine the influence of the intervention, by interpreting the contrast patterns between the temporal observations from control and experimental groups (i.e., paired multivariate time series (PMTS)). Due to recent technological advances and the growing popularity of sensing technology such as in-vehicle sensors and activity trackers, time series data is experiencing explosive growth in both size and complexity. This is threatening to overwhelm the interpretation of control experiments, which conventionally rely on human analysts. Thus, it is imperative to develop automated methods that are expected to simultaneously characterize and detect the interpretable contrast patterns in PMTS generated by controlled experiments. However, there are a few challenges to prohibit existing methods directly addressing this problem: 1) handling the coupling of contrast identification and pattern characterization; 2) dynamically characterizing the patterns in PMTS; 3). Mining the contrast patterns in multiple PMTSs with ubiquitous individual differences. Therefore, we propose a novel framework to mine interpretable contrast patterns based on the dynamic feature dependencies for PMTS through optimization. The proposed framework simultaneously characterizes the dynamic feature dependency networks for PMTS and detects the contrast patterns. Specifically, we characterize the generative process of PMTS as a probabilistic model defined by pairwise Markov random fields whose likelihood are maximized using our group graphical lasso. The model is then generalized to handle multiple PMTSs and solved by proposing a customized algorithm based on the expectation-maximization framework. Extensive experiments demonstrate the effectiveness, scalability, and interpretability of our approach.

Additional Key Words and Phrases: contrast pattern, dynamic feature dependency, controlled experiment, driving behavior, multivariate time series

1 INTRODUCTION

Controlled experiments, which are also known as randomized experiments and A/B tests, are widely used in many domains such as medicine [van Geffen et al. 2011], biology [Agrawal and Kotanen 2003] , etc. Their primary purpose

Authors' addresses: Qingzhe Li, George Mason University, 4400 University Drive, Fairfax, VA, 22030, USA, qli10@gmu.edu; Liang Zhao, George Mason University, 4400 University Drive, Fairfax, VA, 22030, USA, lzhao9@gmu.edu; Yi-Ching Lee, George Mason University, 4400 University Drive, Fairfax, VA, 22030, USA, ylee65@gmu.edu; Jessica Lin, George Mason University, 4400 University Drive, Fairfax, VA, 22030, USA, jessica@gmu.edu.

is to identify and interpret possible differences caused by the intervention between control and experimental groups. In controlled experiments, the multivariate time series generated from the control group usually needs to be exactly paired with the multivariate time series generated from the experimental group. Here we call the control multivariate time series and experimental multivariate time series altogether as paired multivariate time series (PMTS). In this paper, we focus on quantitatively analyzing the effects of an intervention (e.g., alcohol, medicine) on drivers' driving behaviors through the PMTS data.

Driving behavior can be sensed by in-vehicle sensors such as brake or steering wheel positions, and jointly characterized by them via their dependency network. For instance, as shown in Figure 1, whenever a driver is turning, the "steering wheel" sensor will likely have higher values along with slowly decreased values on "velocity" sensor and zero values on both sensors of "brake" and "gas" pedals. These patterns can be summarized by a unique structural pattern of the dependency network as shown in the table in Figure 1. On the other hand, both "steering wheel" and "gas pedal" will have very small or zero values and the "brake" will have higher values with steep decreasing values on "velocity" while slowing down, which are summarized by another structural pattern shown in Figure 1. These structural patterns should be shared by all drivers under all conditions if they try to drive safely. In order to know the effect of the intervention on the driving behavior, a driver is asked to drive twice with and without intervention on exactly the same route under identical traffic environment (i.e., the control factors), so she/he should experience the same sequence of latent driving states (e.g., corresponding to curves, stop signs, etc.) as shown in Figure 1. Hence although cross the controlled and experimental time series, the structural patterns of the dependency networks, the strengths of dependencies could be changed by the intervention. For example, as the dependency networks shown in the "turning" column of the table in Figure 1, the dependency between "steering wheel" and "velocity" is weaker, indicating a lower capability of adjusting the steering wheel according to the "velocity" caused by drinking alcohol. In addition, the driver may still be unaffected by the alcohol for some turns but affected for other turns. For example, because alcohol can increase the probability of making a bad turn, but it is unlikely to guarantee to make bad turns for all turning states. Therefore, the research goal of this paper is to automatically identify whether and how much the intervention makes a difference in causing some "contrast driving behaviors" under the same sequence of latent driving states.

Traditionally, identifying and comparing the patterns in small-scale controlled experiments is accomplished manually [Abou-Zeid et al. 2011]. However, in recent years, huge improvements in sampling rates, as well as the number of available sensors, make manual inspection infeasible. The controlled experiment described above contains millions of time points, tens of participants and an exponential number of node combinations in the dependency networks. This is typical for PMTSs in controlled experiments, which tend to increase rapidly in terms of their data size and complexity, quickly going far beyond the capacity of data analysts using traditional statistics to process or interpret directly. It is therefore imperative to develop new techniques capable of automatically 1) recognizing and characterizing the driving states (e.g., turning) by learning the dynamic dependency networks in PMTS, and 2) discovering contrast patterns in PMTS for each driving state.

Although some previous works are partially related to our problem such as time series subsequence clustering [Goldin et al. 2006; Hallac et al. 2017b], time series segmentation [Matsubara et al. 2014], and contrast pattern mining [Lee et al. 2017; Liu et al. 2017], none of them can simultaneously handle both of the above-mentioned subproblems for PMTS. Several challenges prevent the existing work from being directly utilized or combined to handle this problem: **1) Difficulty in the coupling of latent states characterization and contrast patterns mining for PMTS.** Contrast pattern needs to be discovered by examining the learned dependency network pair for each latent state. Conversely, the strategies for learning dependency networks must be adjusted according to whether the contrast pattern exists or
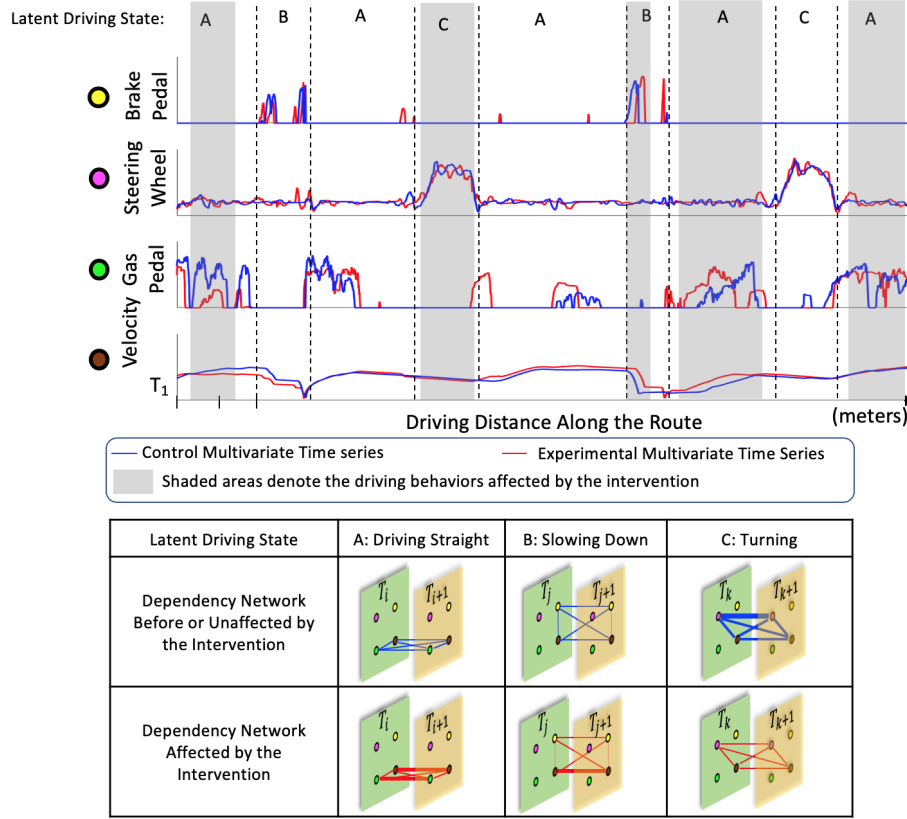
Fig. 1. The contrast patterns in PMTS: the PMTS are plotted at the top. Both time series in the PMTS correspond to the same route with identical traffic conditions as control factors. So they should experience the same driving state at all locations. The unaffected and affected dependency networks corresponding to three latent driving states are plotted at the bottom. The node in the dependency network denotes the same-colored sensor within a small sliding window (i.e., size=2). The widths of the edges denote the strengths of the dependencies between the connected sensors. (better seen in color).

not. The patterns learned by existing works that address the first and second subproblems separately cannot maintain the consistency and optimality of learning; **2) Difficulty in joint dynamic dependency networks learning for PMTS.** As Figure 1 shows, the dependency networks for a common latent state should always share a unique structural pattern, but adding this constraint typically leads to non-convex problem when learning the dependency networks; **3) Difficulty in jointly learning multiple PMTSs.** In controlled experiments, domain experts usually need to see contrast patterns with statistical significance in a group of individuals. There is a big challenge of eliminating the contingency caused by the ubiquitous individual differences when detecting the shared contrast pattern.

To simultaneously address the above challenges, we propose a novel framework to mine the contrast patterns of dynamic dependency networks for PMTS with interpretability. The main contributions of this paper are as follows:

- **Developing a novel framework to mine contrast patterns in the dynamic dependency networks of the PMTS.** A novel CDFD pattern mining problem for PMTS is formulated that simultaneously optimizes latent state recognition and characterization, and CDFD pattern detection problems.

- **Proposing a new group graphical lasso based on a probabilistic model of PMTS.** We creatively model the subsequence pairs in PMTS as multiple Gaussian Markov Random Field (MRF) pairs to simultaneously capture the identical conditional dependency structures and contrast the patterns in each MRF pair. To achieve this, a new group graphical lasso is proposed by adding an $L_{2,1}$-norm regularization term to our probabilistic model.

- **Generalizing the proposed graphical lasso to mine the shared contrast patterns in multiple PMTSs.** To mine the meaningful contrast pattern among multiple PMTSs without contingency caused by the individual differences, we extend the proposed group graphical lasso model from one PMTS to multiple PMTSs. To the best of our knowledge, this model is the first unified model that can simultaneously mine the shared contrast patterns and eliminate the influences of individual differences.

- **Developing an efficient algorithm to solve a new non-convex and non-continuous optimization problem.** To optimize the proposed model, which contains both non-convex and discrete terms, we propose a new algorithm based on Expectation-Maximization (EM) [Dempster et al. 1977] and the Alternating Direction Method of Multipliers (ADMM) [Boyd et al. 2011] that solves the proposed model efficiently and is guaranteed to converge to a locally optimal solution.

- **Conducting comprehensive experiments to validate the effectiveness, efficiency, robustness and interpretability of our proposed approach.** Extensive experiments on 8 synthetic datasets demonstrate the effectiveness, scalability and robustness of the proposed models and algorithms. The experiments on two real-world datasets qualitatively demonstrate the effectiveness and interpretability of the proposed methods on the mined CDFDs.

The rest of this paper is organized as follows. Section 2 reviews the related work. Section 3 formulates the problem of CDFD pattern mining for PMTS. Section 4 presents two models to mine CDFD patterns in one and multiple PMTSs, respectively. Our optimization algorithms are elaborated in Section 5. In Section 6, Extensive experiments are conducted to evaluate the effectiveness, scalability and interpretability of the proposed models and algorithms. The entire work is summarized and concluded in Section 7.

2 RELATED WORK

The previous work related to the research presented in this paper is summarized below.

Contrast pattern mining for time series: There are only a few works on contrast pattern mining for time series which can be divided into two categories: distance-based contrast patterns and model-based contrast patterns. For distance-based contrast patterns that are defined based on some time series distance measures. For example, Lin and Keogh extended the notion of contrast sets for time series which identified the subsequence that differentiates two time series [Lin and Keogh 2006] based on Euclidean distance. Other distance-based contrast patterns in times series such as shapelets [Ye and Keogh 2009] and Representative Patterns [Wang et al. 2016] are developed exclusively for supervised learning tasks. Unlike CDFD pattern, their definitions are all based on some distance measure. However, methods based on such definitions are unable to identify and interpret latent states in controlled experiments. For model-based contrast patterns, a few researchers have begun to utilize multivariate time series generated in fMRI to mine the contrast patterns by proposing various network inference models [Lee et al. 2017; Liu et al. 2017]. For instances, Lee et al. proposed a CNN based deep neural network [Lee et al. 2017] to identify contrasting dependency networks inferred from the entire time series without considering the contrast pattern occurred in subsequence level under common latent state. Similarly, Liu et al. proposed a contrast graphical lasso model [Liu et al. 2017] for whole time series that derives a single contrast dependency network that corresponds to two groups of time series. However, neither of these methods is able to explicitly identify subsequence pairs in PMTS with CDFD patterns.

Table 1. Notations

Notations	Descriptions
m	the count of observations in a multivariate time series
n	the dimensionality of each observation.
C	multivariate time series data C
w	window size parameter
X	one control multivariate time series
$\hat{X}$	one experimental multivariate time series
$(X, \hat{X})$	one PMTS
$(\mathcal{X}, \hat{\mathcal{X}})$	multiple PMTSs
P	the count of PMTS in $(\mathcal{X}, \hat{\mathcal{X}})$
$\theta_k, \hat{\theta}_k$	one pair of MRFs of the kth latent state to be learned
$\Theta^{(k)}, \hat{\Theta}^{(k)}$	P pairs of MRFs of the kth latent state to be learned
Y	latent state assignments to be learned
Z	contrast pattern indicator to be learned
K	the parameter of the latent state count
β	the penalty parameter of switching between contrast and non-contrast latent states
γ	the penalty parameter of switching among different latent state
λ	regularization parameter that controls the sparsity level in the MRFs
ρ	ADMM penalty parameter
$U, \hat{U}$	scaled dual variables in ADMM algorithm

Time series subsequence clustering: mining CDFD pattern requires identifying the latent states in PMTS that could be achieved by clustering the subsequences of PMTS. Clustering all overlapped time series subsequences produces meaningless results [Keogh et al. 2003] due to the reuse of the data points in the overlapping subsequences. Since then, some meaningful distance-based approaches are proposed which avoided the above pitfall. For example, Rakthanmanon et al. proposed a parameter-free Minimum Description Length framework to meaningfully cluster time series subsequences by ignoring some data [Rakthanmanon et al. 2012]. The distance-based approaches cluster time series subsequences by their "shapes," as opposed to our dependency-base patterns. There are also model-based time series subsequence clustering approaches such as those based on ARMA [Xiong and Yeung 2004], Gaussian Mixture model (GMM) [Banfield and Raftery 1993] and Hidden Markov models [Smyth 1997]. These typically consider the whole sequence except for Toeplitz Inverse Covariance-based Clustering (TICC) [Hallac et al. 2017b], proposed recently by Hallac et al., which clusters the subsequences in a single multivariate time series according to structural patterns estimated by a graphical lasso. However, TICC only focuses on single time series, and can neither take into account the correlations among pairs of time series nor mine their contrast patterns.

Graphical lasso for time series: The graphical lasso [Friedman et al. 2008] is validated as an effective and efficient approach for structural learning in Gaussian Markov random fields [Rue and Held 2005] defined by a sparse inverse covariance matrix. Many graphical lasso based models have been applied to time series sparse inverse covariance matrix estimation problems [Hallac et al. 2017a,b; Jung et al. 2015; Veeriah et al. 2015; Yuen et al. 2018], some of which estimated sparse Gaussian inverse covariance matrices for multivariate time series subsequences [Hallac et al. 2017a,b], although they are only able to detect the "latent states" but did not consider the contrast patterns. Others [Jung et al. 2015; Veeriah et al. 2015; Yuen et al. 2018] estimated sparse Gaussian inverse covariance matrices across the entire sequences of multiple univariate time series or one multivariate time series. Jung et al. proposed a graphical model selection scheme based on graphical lasso for stationary time series [Jung et al. 2015], but they applied the graphical lasso to the entire time series which also failed to capture the contrast patterns on subsequence level under common latent state required by the controlled experiments.

$$C = \begin{bmatrix} | & | & & | \\ C_1 & C_2 & \cdots & C_m \\ | & | & & | \end{bmatrix} \xrightarrow[\text{window of size } w]{\text{extract by a sliding}} X = \begin{bmatrix} \text{---} X_1 \text{---} \\ \text{---} X_2 \text{---} \\ \bullet \\ \bullet \\ \bullet \\ \text{---} X_T \text{---} \end{bmatrix}$$

$$\text{where} \quad X_t = \left(\overbrace{\text{--} C_t \text{--}}^{n\text{-dimension}} \quad \overbrace{\text{--} C_{t+1} \text{--}}^{n\text{-dimension}} \quad \bullet \bullet \bullet \quad \overbrace{\text{--} C_{t+w-1} \text{--}}^{n\text{-dimension}} \right)$$
$$\underbrace{}_{n*w\text{-dimension}}$$

Fig. 2. Multivariate Time Series Data Representation

3 PROBLEM SETUP

In this section, we first define the relevant concepts and then present the new problem of contrast dynamic feature dependency pattern mining for PMTS. The key notations, with brief descriptions, are listed in Table 1.

Consider the multivariate time series shown in Figure 2. A multivariate time series $C = [C_1, C_2, \cdots, C_m]$ is a time-ordered sequence of m vectors where each time point $C_t \in \mathbb{R}^{n \times 1}$ is a multivariate observation that contains n dimensions. Unlike the data that follows independent and identically distributed (iid) assumption, the observation of a time point t is also dependent on its context, which is captured by the *subsequences*. Given a sliding window of size $w \ll m$, we define a multivariate time series *subsequence* $X_t \in \mathbb{R}^{1 \times nw}$ as $X_t = [C_t^\mathsf{T}, \ldots, C_{t+w-1}^\mathsf{T}]$ which consists of concatenation of w consecutive n-d vectors starting from the tth time point. We call each dimension in X_t as a *feature*, so there are nw features in X_t. Next, we denote $X = [X_1^\mathsf{T}, X_2^\mathsf{T}, \ldots, X_T^\mathsf{T}]^\mathsf{T}$ which stacks all subsequences of size w in C, where $X \in \mathbb{R}^{T \times nw}$ and $T = m - w + 1$ is the count of subsequences in C. For any given w, there is a one-to-one mapping relationship between C and X, so we will directly use X to denote a multivariate time series in this paper.

In multivariate time series, the sensors in each dimension can be correlated to each other, and neighboring data points of the same dimension have temporal dependency. Therefore, these dependencies may exist between any two features. The structural pattern of the feature dependency network exclusively characterizes a *latent state* as seen in Figure 1, and a multivariate time series data X can be generated from K latent states (e.g. turning, slowing down, and etc.) , where the parameter K is determined by users. Naturally, the feature dependency pattern of each latent state is characterized by a Markov Random Field (MRF) [Kindermann and Snell 1980] among the nw features in X. Specifically, we denote $G_k = (X_t, \theta_k)$ as the Gaussian MRF which generates the subsequences belonging to the kth latent state, where $\theta_k \in \mathbb{R}^{nw \times nw}$ is the inverse covariance matrix that defines G_k and encodes the structural representation of the conditional independency among the features. We use $Y \in \{0, 1\}^{T \times K}$ to denote the assignments of the latent state for all time points. Specifically, $Y_{t,k} = 1$ if X_t belongs to the kth latent state, otherwise, $Y_{t,k} = 0$.

In controlled experiments, time series commonly come in pairs, so the *paired multivariate time series* is formally defined as:

Definition 3.1 (Paired Multivariate Time Series (PMTS)). We denote two multivariate time series as X and $\hat{X}$, where X is defined as *control time series* and $\hat{X}$ is the *experimental time series* of X such that: 1) X and $\hat{X}$ have the same size T (i.e., the count of subsequences for a given w), 2) each pair of X_t and $\hat{X}_t$ shares the same assignment of latent state Y_t,

and 3) for all $k = 1, \cdots, K$, their k^{th} latent states are always identical in their conditional independency structure such that: $\text{supp}(\theta_k) = \text{supp}(\hat{\theta}_k)$, where the matrix support "supp" is defined as the index set of nonzero elements.

For the example shown in Figure 1, two time series in PMTS contain the same count of subsequences for a given w, and the subsequences in the same road segment are defined to share the same latent state (e.g., turning) assignments. Here we do not define our contrast pattern by comparing the differences between the actual driving states with and without the intervention. Instead, we define our contrast pattern as the differences in the dependency strengths by assuming both drives share the same latent state assignments. Formally, our contrast dynamic feature dependency pattern is defined as follows:

Definition 3.2 (Contrast Dynamic Feature Dependency (CDFD)). Given a PMTS $(X, \hat{X})$, for each subsequence pair $(X_t, \hat{X}_t)$ where $t = 1, \ldots, T$, a *Contrast Dynamic Feature Dependency (CDFD)* pattern exists if, and only if X_t and $\hat{X}_t$ are generated from different MRFs defined by θ_k and $\hat{\theta}_k$, where $\text{supp}(\theta_k) = \text{supp}(\hat{\theta}_k)$ and $\theta_k \neq \hat{\theta}_k$. The existences of the CDFD patterns are denoted by a *contrast indicator* $Z \in \{0, 1\}^{T \times 1}$. Specifically, $Z_t = 0$ when there is CDFD pattern between X_t and $\hat{X}_t$, and $Z_t = 1$ when there is no CDFD pattern (i.e., X_t and $\hat{X}_t$ are generated from identical MRFs).

For example, as the dependency networks shown in the bottom of Figure 1, the CDFD pattern refers to the characterization of the dependency networks θ_k and $\hat{\theta}_k$ (i.e., within each column or latent state) which have the identical structural pattern but different feature dependency strengths. To capture the fact that the intervention (e.g. alcohol) is likely to increase the probability of the occurrences of CDFD patterns but unlikely to guarantee the occurrences of CDFD patterns, we define the problem in a more general way by introducing the contrast indicator Z that to be learned from PMTS. Our assumption is weaker since we do not enforce all the instances to have contrast patterns presumably but learn the patterns from the data. The problem of the *Contrast Dynamic Feature Dependency pattern mining for one PMTS* is formulated as follows:

Problem Formulation: Given a PMTS $(X, \hat{X})$, our goal is to mine its interpretable CDFD patterns, which requires to: 1) characterize the K latent states by learning their MRFs $\theta = \{\theta_k\}_k^K$ and $\hat{\theta} = \{\hat{\theta}_k\}_k^K$, 2) determine the latent state assignments Y, and 3) decide the Z assignments by detecting the CDFD pattern for each subsequence.

For the example in Figure 1, given a PMTS $(X, \hat{X})$ obtained from the driving simulator without (i.e., X) and with (i.e., $\hat{X}$) an intervention, mining the CDFD patterns involves to: 1) characterize the K driving states encoded by θ and $\hat{\theta}$, 2) determine the driving state assignments Y for all the road segments, and 3) decide the Z assignments based on whether the driving behaviors have been changed for each road segment.

The above problem poses the following main technical challenges: (1) *Difficulty in jointly learning all the variables* $\theta_k, \hat{\theta}_k, Y, Z$ *for each PMTS*. These variables are correlated with each other and thus must be jointly learned. However, there is no existing model that can jointly characterize them in a unified framework. (2) *Difficulty in maintaining the dependencies among the paired MRFs in PMTS*. As stated in Definition 3.1, the constraint requiring identical patterns for the conditional independence structures between the MRFs in each latent state, namely $\text{supp}(\theta_k) = \text{supp}(\hat{\theta}_k)$, must be protected during the parameter optimization process. This constraint is inherently non-convex, which is difficult to maintain effectively and efficiently during the optimization process.

4 METHODOLOGY

The models of mining CDFD pattern in PMTS are proposed in this section: we first propose a new probabilistic modeling method for PMTS in Section 4.1. Then a novel model of CDFD pattern Mining for PMTS (CMP) is proposed to mine

the CDFD in one PMTS in Section 4.2. The CMP model is generalized to Group CMP (GCMP) model which mines the CDFD in multiple PMTSs in Section 4.3.

4.1 Probabilistic Modeling of PMTS

As X_t and $\hat{X}_t$ are continuous variables, they are defined to be sampled from multivariate-Gaussian distributions. When $Z_t = 0$ (i.e., existing CDFD), X_t and $\hat{X}_t$ are generated from the multivariate-Gaussian distributions defined by different inverse covariance matrices θ_k and $\hat{\theta}_k$, respectively: $X_t \sim \mathcal{N}(X_t|\theta_k, \mu_k)$ and $\hat{X}_t \sim \mathcal{N}(X_t|\hat{\theta}_k, \hat{\mu}_k)$ such that the conditional joint distribution of $(X_t, \hat{X}_t)$ is:

$$p(X_t, \hat{X}_t|Y_{t,k} = 1, Z_t = 0) = \mathcal{N}(X_t|\theta_k, \mu_k) \cdot \mathcal{N}(\hat{X}_t|\hat{\theta}_k, \hat{\mu}_k). \tag{1}$$

Otherwise, when $Z_t = 1$, X_t and $\hat{X}_t$ are generated from the multivariate-Gaussian distributions defined by the same inverse covariance matrix $\Theta^{(k)}$: $X_t \sim \mathcal{N}(X_t|\theta_k, \mu_k)$ and $\hat{X}_t \sim \mathcal{N}(X_t|\theta_k, \hat{\mu}_k)$ such that the conditional joint distribution of $(X_t, \hat{X}_t)$ is:

$$p(X_t, \hat{X}_t|Y_{t,k} = 1, Z_t = 1) = \mathcal{N}(X_t|\theta_k, \mu_k) \cdot \mathcal{N}(\hat{X}_t|\theta_k, \hat{\mu}_k). \tag{2}$$

Based on above equations, for all the time points $t = 1, \cdots, T$, the likelihood of $(X, \hat{X})$ conditioned on the parameters Y, Z, θ, and $\hat{\theta}$ is:

$$p(X, \hat{X}|Y, Z, \theta, \hat{\theta}) \quad = \quad \prod_{k,t}^{K,T} [\mathcal{N}(X_t|\theta_k, \mu_k)^{Y_{t,k}} \mathcal{N}(\hat{X}_t|\theta_k, \hat{\mu}_k)^{Y_{t,k}}]^{Z_t} [\mathcal{N}(X_t|\theta_k, \mu_k)^{Y_{t,k}} \mathcal{N}(\hat{X}_t|\hat{\theta}_k, \hat{\mu}_k)^{Y_{t,k}}]^{(1-Z_t)} \tag{3}$$

4.2 CDFD Pattern Mining for One PMTS

This section presents our proposed model of *Contrast dynamic feature dependency pattern Mining for one PMTS (CMP)*, which optimizes the parameters of the probabilistic model for a single PMTS. To achieve this, three considerations must be taken into account: 1) the maximal likelihood of the probabilistic model for PMTS; 2) regularization on the structure of the paired MRFs for PMTS; and 3) the temporal dependency of the latent state assignments. These are discussed in turn below.

4.2.1 Loss function. Given a PMTS $(X, \hat{X})$, maximizing the likelihood of Equation (3) is equivalent to minimizing the negative log likelihood, leading to our loss function:

$$\mathcal{L}(Y, Z, \theta, \hat{\theta}) = \sum_{t,k}^{T,K} Y_{t,k}[Z_t(-\ell\ell(X_t, \theta_k) - \ell\ell(\hat{X}_t, \theta_k)) + (1 - Z_t)(-\ell\ell(X_t, \theta_k) - \ell\ell(\hat{X}_t, \hat{\theta}_k))] \tag{4}$$

where $\ell\ell(A, B) = -\frac{1}{2}(A - \mu)^{\mathsf{T}}B(A - \mu) + \frac{1}{2}\log\det B - \frac{n}{2}\log(2\pi))$ denotes the log likelihood that the multivariate subsequence A comes from the Gaussian distribution with inverse covariance matrix B.

4.2.2 Structural and temporal regularization. Due to the identical conditional independency structure constraint required in Definition 1, the widely used L_1-norm regularization term [Hallac et al. 2017b] would not satisfy such constraint. We thus propose an $L_{2,1}$-norm regularization term which enforces the identical sparsity pattern in the contrast MRF pair defined by θ_k and $\hat{\theta}_k$, so the zero values correspond to the conditional independent relationship between the two features. Our $L_{2,1}$-norm regularization term is defined as: $\sum_k^K \|\lambda \cdot [v(\theta_k), v(\hat{\theta}_k)]\|_{2,1}$, where $v(\cdot)$ is a vectorization function for any input matrix, λ is the regularization parameter that determines the sparsity level in the MRFs. To distinguish the dependency patterns for different latent states, the values of λ should be always greater than zero since $\lambda=0$ will lead to a clique for all MRFs, and should not be too large as this will cause some learned θ_k and $\hat{\theta}_k$

are both equal to **0**. Typically, any λ value between 0.1 to 50 works well for normalized PMTS.

Due to the nature of temporal continuity in time series, neighboring points tend to have consistent latent state assignments as suggested in "Toeplitz Inverse Covariance-Based Clustering of Multivariate Time Series Data" (TICC) [Hallac et al. 2017b]. In addition, the contrast pattern has temporal dependency as well. We thus penalize the divergence between neighboring time points on both the Y and Z assignments by proposing the following smoothing term:

$$\boldsymbol{h}_{\beta,\gamma}(Y,Z) = \sum_t^T (\beta \mathbb{1}(Z_t \neq Z_{t-1}) + \gamma \mathbb{1}(Y_t \neq Y_{t-1}))$$

where $\mathbb{1}(\cdot)$ is an indicator function that maps "True" values to 1 and "False" values to 0, β is the penalty if $Z_t \neq Z_{t-1}$ and γ is the penalty of switching among the K latent states. Typically, setting β and γ to any values between 0 and 50 will work for z-normalized PMTS.

4.2.3 Objective function. Based on the loss function and the regularization terms proposed above, our overall objective function is to jointly minimize them all:

$$\underset{Y,Z,\{\theta,\hat{\theta}\}>0}{\arg\min} \sum_k^K \|\lambda \circ [v(\theta_k), v(\hat{\theta}_k)]\|_{2,1} + \boldsymbol{h}_{\beta,\gamma}(Y,Z) + \mathcal{L}(Y,Z,\theta,\hat{\theta}).$$

In addition to the regularization parameters λ, β and γ discussed in Section 4.2.2, K and w can be chosen based on prior knowledge, through cross validation, or by a principled method such as Bayesian information criterion [Schwarz et al. 1978]. If the count of subsequences assigned to any latent state is too small (e.g. less than 30) to learn a good θ_k and $\hat{\theta}_k$, this indicates that the value of K should be decreased. Since the short term temporal dependency is much stronger than the long term temporal dependency in real-world applications, the window size w should be small (e.g. $w < 10$).

4.3 CDFD Pattern Mining for Multiple PMTSs

The CMP model proposed above focuses on discovering the patterns for a single PMTS, but in many situations there are actually multiple PMTSs. For example, when testing an intervention, typically multiple participants will be invited to test for common effects on the population based on all their corresponding PMTSs. And it is required to collectively discover the contrast patterns between control and experimental time series shared by multiple PMTSs.

We therefore focus on mining the collective patterns of multiple PMTSs by generalizing CMP to a new model named *Group CMP (GCMP)*. Given P PMTSs, and all the control time series are denoted as $\mathcal{X} = [\mathcal{X}_1, \cdots, \mathcal{X}_P]$ while the experimental time series are $\hat{\mathcal{X}} = [\hat{\mathcal{X}}_1, \ldots, \hat{\mathcal{X}}_P]$. For each PMTS $(\mathcal{X}_p, \hat{\mathcal{X}}_p)$, $\hat{\mathcal{X}}_p$ is the experimental time series corresponding to its control $\mathcal{X}_p$. We denote $\Theta_p^{(k)}$ and $\hat{\Theta}_p^{(k)}$ as the contrast inverse covariance matrices of the kth latent state, where $k = 1, \ldots, K$, $p = 1 \ldots, P$ and define $\Theta = \{\Theta_p^{(k)}\}_{p,k}^{P,K}$ and $\hat{\Theta} = \{\hat{\Theta}_p^{(k)}\}_{p,k}^{P,K}$, in order to discover shared patterns across multiple PMTSs, the same latent state assignment and the contrast indicator must be shared by all the P pairs, and are thus still denoted as Y and Z, respectively. Moreover, as the conditional independencies of the MRFs across all PMTSs share the same structure, for any two different pairs p and q, we have

$$\mathrm{supp}(\Theta_q^{(k)}) = \mathrm{supp}(\Theta_p^{(k)}) = \mathrm{supp}(\hat{\Theta}_p^{(k)}) = \mathrm{supp}(\hat{\Theta}_q^{(k)}). \tag{5}$$

Therefore, the problem of GCMP can be formally defined as follows: given P PMTSs, GCMP: 1) characterizes the MRFs $\Theta_p^{(k)}$ and $\hat{\Theta}_p^{(k)}$ for each state K and each pair p, 2) detects the shared latent state assignment Y, and 3) identifies the unified contrast indicator Z.

The loss function for P PMTSs can be generalized from the loss function for one PMTS defined in Equation (4): $\sum_p^P \mathcal{L}(Y, Z, \Theta_p, \hat{\Theta}_p)$. As defined in Equation (5), the MRFs for different PMTS share the same sparsity pattern, enabling us to propose a new group-based regularization term to enforce the identical sparcity pattern on all $\Theta_p^{(k)}$ and $\hat{\Theta}_p^{(k)}$ such that : $\sum_k^K g(\Theta^{(k)}, \hat{\Theta}^{(k)})$ where

$$g(\Theta^{(k)}, \hat{\Theta}^{(k)}) = \|\lambda \circ [v(\Theta_1^{(k)}), v(\hat{\Theta}_1^{(k)}), \ldots, v(\Theta_P^{(k)}), v(\hat{\Theta}_P^{(k)})]\|_{2,1}$$

Finally, imposing a similar penalty over the latent state assignment Y and contrast indicator Z also enforces their temporal continuity. The overall objective function for the GCMP problem can now be defined as:

$$\underset{Y, Z, \Theta, \hat{\Theta}}{\arg\min} \sum_k^K g(\Theta^{(k)}, \hat{\Theta}^{(k)}) + \boldsymbol{h}_{\beta, \gamma}(Y, Z) + \sum_p^P \mathcal{L}(Y, Z, \Theta_p, \hat{\Theta}_p) \tag{6}$$

Comparing the objective function in Equation (6) for GCMP with the objective function introduced in Section 4.2.3 for CMP reveals that the GCMP model is actually the generalization of the CMP model and that when $P = 1$, GCMP reduces to CMP.

4.4 Relationship to the related state-of-the art approach

In this section, we show that the current state-of-the-art approach, the TICC [Hallac et al. 2017b] model, is actually a special case of the proposed model.

The TICC approach is only able to solve the second subproblem defined in Section 3 (i.e., determine the latent state assignment Y). In the proposed CPM model, let $Z_t = 1$ for all $t = 1, \ldots T$, which means there is no contrast pattern allowed, the model is thus reduced to the TICC model:

$$\underset{Y, \theta > 0}{\arg\min} \sum_{t,k}^{T,K} Y_{t,k}[-\ell\ell(X_t, \theta_k) - \ell\ell(\hat{X}_t, \theta_k)] + \sum_t^T \gamma \mathbb{1}(Y_t \neq Y_{t-1}) + \sum_k^K \|\lambda \circ v(\theta_k)\|_1$$

However, it would not be able to mine the contrast pattern anymore.

5 PARAMETER OPTIMIZATION

In this section, the parameter optimization algorithm for GCMP is presented and its special case CMP solved by simply setting $P = 1$ in our algorithm. Equation (6) is a mixture of the combinational optimization of discrete variables (i.e., Y, Z) and non-convex nonsmooth optimization of continuous variables (i.e., $\Theta, \hat{\Theta}$). As there is no existing algorithm capable of solving this problem efficiently and effectively, we propose a new algorithm based on Expectation-Maximization (EM) [Moon 1996] and the Alternating Direction Method of Multipliers (ADMM) [Boyd et al. 2011]. The details are summarized in Algorithm 1 that alternately optimize the continual variables and discrete variables until stationary. The maximization step (M-step) described in Lines 3-17 jointly optimizes Θ and $\hat{\Theta}$ by adapting the ADMM framework; the expectation step (E-step) is performed in Line 18. The M-step and E-step are described in more detail in Section 5.1 and 5.2, respectively.

Algorithm 1 Parameter Optimization for GCMP

Require: X, $\hat{X}$, λ, β, γ, w
Ensure: solution Y, Z, Θ, $\hat{\Theta}$
1: **repeat**
2:     **for** $K = 1$ to K **do**
3:         initialize Θ, $\hat{\Theta}$, Q, $\hat{Q}$, U, $\hat{U} \leftarrow \mathbf{0}$
4:         **repeat**
5:             **for** $p = 1$ to P **do**
6:                 $\Theta_p^{(k)} \leftarrow$ Equation (9)   // update $\Theta_p^{(k)}$
7:                 $\hat{\Theta}_p^{(k)} \leftarrow$ Equation (10)   //update $\hat{\Theta}_p^{(k)}$
8:             **end for**
9:             **for** $i = 1$ to nw **do**
10:                 **for** $j = 1$ to i **do**
11:                     $[Q_{0,i,j}^{(k)}, \hat{Q}_{0,i,j}^{(k)}] \leftarrow$ Equation (11)   //update the lower entries
12:                     $[Q_{0,j,i}^{(k)}, \hat{Q}_{0,j,i}^{(k)}] \leftarrow [Q_{0,i,j}^{(k)}, \hat{Q}_{0,i,j}^{(k)}]$ //make the matrices symmetric
13:                 **end for**
14:             **end for**
15:             $U^{(k)}, \hat{U}^{(k)} \leftarrow$ Equation (12)
16:         **until** convergence
17:     **end for**
18:     E-step: optimizing Y and Z is described in Section 5.2
19: **until** Y and Z assignments are stationary

5.1 M-step: Optimizing $\Theta^{(k)}$ and $\hat{\Theta}^{(k)}$

5.1.1 Decomposing GCMP into K subproblems: In the "M-step", we fix the latent state assignment Y and contrast indicator Z, and optimize $\Theta^{(k)}, \hat{\Theta}^{(k)}$ in parallel, for all K latent states. We therefore rewrite the joint likelihood term as:

$$\sum_p^P \mathcal{L}(Y, Z, \Theta_p, \hat{\Theta}_p) = \sum_{k=1}^K \sum_{p=1}^P (f(\Theta_p^{(k)}) + \hat{f}(\hat{\Theta}_p^{(k)})) + CONST \tag{7}$$

where

$$f(\Theta_p^{(k)}) = \frac{1}{2}[|\mathcal{X}_p^{(k,1)}|tr(S(\mathcal{X}_p^{(k,1)})\Theta_p^{(k)}) + |\hat{\mathcal{X}}_p^{(k,1)}|tr(S(\hat{\mathcal{X}}_p^{(k,1)})\Theta_p^{(k)}) +$$

$$|\mathcal{X}_p^{(k,0)}|tr(S(\mathcal{X}_p^{(k,0)})\Theta_p^{(k)}) - (|\mathcal{X}_p^{(k,1)}| + |\hat{\mathcal{X}}_p^{(k,1)}| + |\mathcal{X}_p^{(k,0)}|)\log\det\Theta_p^{(k)}]$$

$$\hat{f}(\hat{\Theta}_p^{(k)}) = \frac{1}{2}|\hat{\mathcal{X}}_p^{(k,0)}|[tr(S(\hat{\mathcal{X}}_p^{(k,0)})\hat{\Theta}_p^{(k)}) - \log\det\hat{\Theta}_p^{(k)}]$$

Here P is the count of PMTSs; $\mathcal{X}_p^{(k,z)} \in \mathbb{R}^{c \times nw}$ is the matrix which stacks all the subsequences belonging to the kth latent state with (i.e., $z = 0$) or without (i.e., $z = 1$) CDFD in $\mathcal{X}_p$, where $c = |\mathcal{X}_p^{(k,z)}|$ is the count of these subsequences. $tr(\cdot)$ is the trace of the matrix and $S(\cdot)$ is a function that computes the empirical covariance matrix: $S(A) = \frac{1}{|A|}\sum_{r=1}^{|A|} A_r A_r^\mathsf{T}$.

According to Equation (7), Equation (6) can be optimized separately for each pair of covariances $(\Theta^{(k)}, \hat{\Theta}^{(k)})$ to formulate a graphical lasso problem [Friedman et al. 2008]:

$$\underset{\{\Theta_p^{(k)}, \hat{\Theta}_p^{(k)}\} > 0}{\arg\min} \quad g(\Theta^{(k)}, \hat{\Theta}^{(k)}) + \sum_p^P (f(\Theta_p^{(k)}) + \hat{f}(\hat{\Theta}_p^{(k)})).$$

5.1.2 Solving Graphical lasso: Solving each graphical lasso problem involves exploring all the sparse patterns for $(nw)^2$ elements, and there are the K graphical lasso problems to be solved dozens of times before the E-M algorithm converges. However, we notice the graphical lasso problem can be solved efficiently by adapting the ADMM framework

after re-formulating into its equivalent form by introducing the consensus variables $Q^{(k)}$ and $\hat{Q}^{(k)}$.

$$\arg\min_{\{Q^{(k)},\hat{Q}^{(k)},\Theta_p^{(k)},\hat{\Theta}_p^{(k)}\}>0} g(\Theta^{(k)},\hat{\Theta}^{(k)}) + \sum_p^P (f(\Theta_p^{(k)}) + \hat{f}(\hat{\Theta}_p^{(k)}))$$

$$s.t., \ Q^{(k)} = \Theta^{(k)}, \hat{Q}^{(k)} = \hat{\Theta}^{(k)}$$

of which the augmented Lagrangian form [Boyd et al. 2011] is:

$$L_\rho(\Theta^{(k)}, \hat{\Theta}^{(k)}, Q^{(k)}, \hat{Q}^{(k)}, U^{(k)}, \hat{U}^{(k)}) = g(Q^{(k)}, \hat{Q}^{(k)})$$

$$+ \sum_p^P (f(\Theta_p^{(k)}) + \hat{f}(\hat{\Theta}_p^{(k)})) - \frac{\rho}{2}\|[U^{(k)}, \hat{U}^{(k)}]\|_F^2 \tag{8}$$

$$+ \frac{\rho}{2}\|[\Theta^{(k)}, \hat{\Theta}^{(k)}] - [Q^{(k)}, \hat{Q}^{(k)}] + [U^{(k)}, \hat{U}^{(k)}]\|_F^2$$

where $\rho > 0$ is the ADMM [Boyd et al. 2011] penalty parameter and U and $\hat{U}$ are the scaled dual variables.

Equation (8) can be solved by iteratively updating $[\Theta, \hat{\Theta}]$, $[Q, \hat{Q}]$ and $[U, \hat{U}]$ until convergence. Due to the convexity of the objective function and the simplicity of the linear equality constraint, the convergence is theoretically guaranteed to the global optimal solution. Each subproblem can be solved as described below:

Updating $\Theta^{(k)}$ and $\hat{\Theta}^{(k)}$: All the P pairs of $\Theta_p^{(k)}$ and $\hat{\Theta}_p^{(k)}$ can be updated in parallel. $\Theta_p^{(k)}$ is updated by solving the following objective function:

$$\arg\min_{\Theta_p^{(k)}} f(\Theta_p^{(k)}) + \frac{\rho}{2}\|\Theta_p^{(k)} - Q_p^{(k)} + U_p^{(k)}\|_F^2,$$

We first set the partial derivative of the target variable $\Theta_p^{(k)}$ to 0, then move the terms with known variables to the right hand side:

$$2\rho\Theta_p^{(k)} - [|\mathcal{X}_p^{(k,1)}| + |\hat{\mathcal{X}}_p^{(k,1)}| + |\mathcal{X}_p^{(k,0)}|]\Theta_p^{(k)^{-1}} = 2\rho(Q_p^{(k)} - U_p^{(k)}) - [|\mathcal{X}_p^{(k,1)}|S(\mathcal{X}_p^{(k,1)}) + |\hat{\mathcal{X}}_p^{(k,1)}|S(\hat{\mathcal{X}}_p^{(k,1)}) + |\mathcal{X}_p^{(0)}|S(\mathcal{X}_p^{(k,0)})]$$

After performing the eigendecomposition on the right hand side of above equation, the solution is:

$$\Theta_p^{(k)} = D\tilde{\Theta}^{(k)}D^\mathsf{T} \tag{9}$$

where the square matrix D and diagonal matrix Λ are the resulting eigenvectors and eigenvalues of the eigendecomposition, respectively. And $\tilde{\Theta}_{p,ii}^{(k)} = (\Lambda_{ii} + \sqrt{\Lambda_{ii}^2 + 8\rho(|\mathcal{X}_p^{(k,1)}| + |\hat{\mathcal{X}}_p^{(k,1)}| + |\mathcal{X}_p^{(k,0)}|)})/4\rho$.

We update $\hat{\Theta}_p^{(k)}$ by solving the objective function:

$$\arg\min_{\hat{\Theta}_p^{(k)}} \hat{f}(\hat{\Theta}_p^{(k)}) + \frac{\rho}{2}\|\hat{\Theta}_p^{(k)} - \hat{Q}_p^{(k)} + \hat{U}_p^{(k)}\|_F^2$$

This can be solved as for $\Theta_p^{(k)}$. The solution is:

$$\hat{\Theta}_p^{(k)} = D\tilde{\hat{\Theta}}^{(k)}D^\mathsf{T} \tag{10}$$

where the square matrix D and the diagonal matrix Λ are obtained by eigendecomposition: $2\rho(\hat{Q}_p^{(k)} - \hat{U}_p^{(k)}) - |\hat{\mathcal{X}}_p^{(k,0)}| \cdot S(\hat{\mathcal{X}}_p^{(0)}) = D\Lambda D^\mathsf{T}$ and $\tilde{\hat{\Theta}}_p^{(k)}$ is the diagonal matrix whose i-th element $\tilde{\hat{\Theta}}_{p,ii}^{(k)}$ on the diagonal is $(\Lambda_{ii} + \sqrt{\Lambda_{ii}^2 + 8\rho|\hat{\mathcal{X}}_p^{(k,0)}|})/4\rho$.
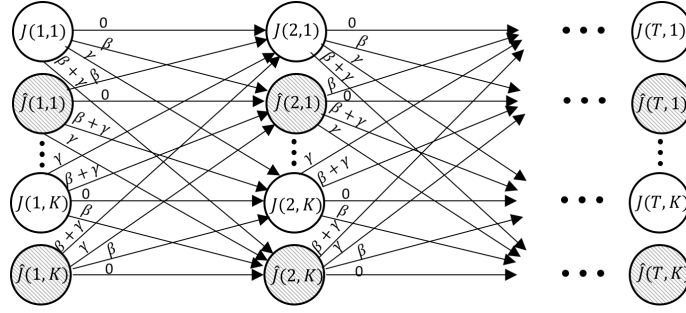
Fig. 3. E-step: optimizing Y and Z assignments can be solved by selecting one node from each layer (i.e., each column) to minimize the amount cost spent on the nodes and edges.

Updating $[Q^{(k)}, \hat{Q}^{(k)}]$: $[Q^{(k)}, \hat{Q}^{(k)}]$ is updated by solving the optimization function:

$$\underset{Q^{(k)}, \hat{Q}^{(k)}}{\arg\min} g(Q^{(k)}, \hat{Q}^{(k)}) + \frac{\rho}{2} \|[\Theta^{(k)}, \hat{\Theta}^{(k)}] - [Q^{(k)}, \hat{Q}^{(k)}] + [U^{(k)}, \hat{U}^{(k)}]\|_F^2$$

This minimization problem can be solved by a group soft thresholding operator [Boyd et al. 2011]:

$$[Q_{0,i,j}^{(k)}, \hat{Q}_{0,i,j}^{(k)}] \leftarrow \eta_{\lambda/rho}([\Theta_{0,i,j}^{(k)}, \hat{\Theta}_{0,i,j}^{(k)}] + [U_{0,i,j}^{(k)}, \hat{U}_{0,i,j}^{(k)}]) \tag{11}$$

Here $B_{0,i,j} \in \mathbb{R}^P$ denotes the vector in a 3rd-order tensor of size $P \times nw \times nw$ where $B \in \{\Theta^{(k)}, \hat{\Theta}^{(k)}, Q^{(k)}, \hat{Q}^{(k)}, U^{(k)}, \hat{U}^{(k)}\}$, $i = 1, 2, \ldots, (nw)$, and $j = 1, \ldots, i$. The group soft-thresholding function [Donoho et al. 1993] is defined as: $\eta_{\lambda/\rho}(\boldsymbol{a}) = (1 - \frac{\lambda}{\rho \|\boldsymbol{a}\|_2})_+ \boldsymbol{a}$.

Updating $[U^{(k)}, \hat{U}^{(k)}]$: $[U^{(k)}, \hat{U}^{(k)}]$ is updated by

$$[U^{(k)}, \hat{U}^{(k)}] \leftarrow [U^{(k)}, \hat{U}^{(k)}] + [\Theta^{(k)}, \hat{\Theta}^{(k)}] - [Q^{(k)}, \hat{Q}^{(k)}] \tag{12}$$

5.2 E-step: Optimizing the Y, Z Assignments

In the E-step, we fix $\Theta^{(k)}$ and $\hat{\Theta}^{(k)}$ for all $k = 1, \ldots, K$, and vary the Y and Z assignment for each index t to minimize

$$\arg\min_{Y,Z} \sum_t^T (\beta \mathbb{1}\{Z_t \neq Z_{t-1}\} + \gamma \mathbb{1}\{Y_t \neq Y_{t-1}\})$$

$$+ \sum_{t,K}^{T,K} Y_{t,k}[Z_t \hat{J}(t,k) + (1 - Z_t)J(t,k)] \tag{13}$$

where $J(t,k) = \sum_p^P (-\ell\ell(X_{p,t}, \Theta_p^{(k)}) - \ell\ell(\hat{X}_{p,t}, \Theta_p^{(k)}))$

and $\hat{J}(t,k) = \sum_p^P (-\ell\ell(X_{p,t}, \Theta_p^{(k)}]) - \ell\ell(\hat{X}_{p,t}, \hat{\Theta}_p^{(k)}))$.

The assignment optimization problem in above equation can be formulated and solved as a classic problem of finding the minimum cost Viterbi path [Viterbi 1967] in a fully connected network, as shown in Figure 3. Each layer/column t represents the index of the series and each row represents a unique Y and Z assignments. For instance, the node $J(t,k)$ denotes the cost of assigning $Y_{t,k}$=1 and Z_t=1, and node $\hat{J}(t,k)$ denotes the cost of assigning $Y_{t,k}$=1 and Z_t=0. The optimization problem in E-step can be solved by finding an optimal path from t=1 to T such that the total cost at the edges and the nodes is minimal, which can be solved by dynamic programming in $O(KT)$ time where the current cost

at each node is updated by:

$$J(t+1, k)= \min(J_{\min}(t)+\gamma, \hat{J}_{\min}(t)+\beta+\gamma, J(t, k), \hat{J}(t, k)+\beta)$$
$$\hat{J}(t+1, k)= \min(\hat{J}_{\min}(t)+\gamma, J_{\min}(t)+\beta+\gamma, \hat{J}(t, k), J(t, k)+\beta)$$

where $J_{\min}(t)$ and $J_{\min}(t)$ are the minimal costs to t-th layer of all J-nodes and all $\hat{J}$-nodes, respectively. Finally, the shortest path through the network from left to right with minimal cost is recovered by backtracking.

6 EXPERIMENTS

The performance of the proposed models is evaluated on 8 synthetic and 13 real-world datasets in Sections 6.1 and 6.2, respectively. All the experiments are conducted on a 64-bit machine with Intel(R) processor (i7CPU@2.5 GHz) AND 16 GB memory.

6.1 Experiments on Synthetic Datasets

6.1.1 *Experimental Setup:* The generation process for the synthetic datasets, the comparison methods used and the parameter settings and evaluation metrics are described in turn below.

Generating the Synthetic Datasets: The process used to generate four group datasets (i.e., Datasets 5-8), where each dataset contains seven PMTSs (i.e.,$P = 7$), is described below. In addition, four individual experimental datasets (i.e., Datasets 1-4) are generated by using the same process by setting $P = 1$. Each dataset is generated for ten times, then the average performance of ten repetitive experiments are reported.

(1) *Generating the inverse covariance matrices Θ and $\hat{\Theta}$:* $\Theta_p^{(k)}$ and $\hat{\Theta}_p^{(k)}$ need to be generated for all $p = 1 \ldots P$ and $k = 1 \ldots K$, where K is the number latent states. To prevent the generated inverse covariance matrices biasing to our model, we follow the generation process described in [Hallac et al. 2017b], which enforces the block Toeplitz constraint on the inverse covariance matrix. Specifically, we generate the inverse covariance matrices in three steps: 1) An unweighted undirected clique with $n = 5$ nodes is created; 2) As described in Figure 1, each latent driving behavior corresponds to a unique sparse structural pattern of its dependency network. To simulate this, $w \cdot K$ unweighted and undirected Erdős-Rényi random graphs $E^{(k,v)}$ [Erdős et al. 2013] are generated by randomly removing 80% edges in the clique, where $w = 5$ is the window size; $v = 1, \cdots, w$; and $k = 1, \cdots, K$. Each removed edge, which reflects the conditional independency in the MRFs between the nodes/features connected, lead to a zero-value of the inverse covariance matrix that encodes the dependency network or MRF. 3) For each random graph $E^{(w,v)}$, P pairs of weighted graphs encoded by adjacent matrices $(\{W_p^{(k,v)}, \hat{W}_p^{(k,v)}\} \in \mathbb{R}^{n \times n})$ that share the identical zero entries, are generated by assigning a random weight to every non-zero entry, which simulates various strengths of the dependencies caused by the individual differences on driving behaviors. and 4) Finally, each pair of the inverse covariance matrices $(\Theta_p^{(k)}, \hat{\Theta}_p^{(k)}$ are generated by constructing a pair of $wn \times wn$ Toeplitz matrices using $(\{W_p^{(k,v)}, \hat{W}_p^{(k,v)}\}$. To ensure inversibility, the values in the generated inverse covariance matrices are adjusted by $\Theta_p^{(k)} = \Theta_p^{(k)} + (0.1 + |e|)I$ and $\hat{\Theta}_p^{(k)} = \hat{\Theta}_p^{(k)} + (0.1 + |\hat{e}|)I$, where e and $\hat{e}$ are the smallest eigenvalues of the corresponding $\Theta_p^{(k)}$ and $\hat{\Theta}_p^{(k)}$, respectively.

(2) *Generating labels for the latent state assignment Y and contrast pattern indicator Z:* To simulate the temporal dependency of the time series in the real world, we first select a sequence of segments for the Y assignments. For example, the sequence of "1,2,1" denotes 3 segments assigned to $K = 2$ latent states, where "1" and "2" denote the Latent States 1 and 2, respectively. Let each segment contain $100 * K$ time points. The latent state assignments $Y_{t,k}$ for $t = 1, \ldots, 200$ would be $Y_{t,1} = 1$, and for $t = 201, \ldots, 400$ and $t = 401, \ldots, 600$ would be $Y_{t,2} = 1$ and $Y_{t,1} = 1$, respectively. Following this rationale, the datasets used in this section are generated from 4 segment sequences: "1,2,1","1,2,3,2,1","1,2,3,4,1,2,3,4"

and "1,2,2,1,3,3,3,1". The datasets for each sequence is generated ten times for repeating the experiments to get the average result. To determine the sequence of the Z assignments, the time points that belong to the 1/4 to 3/4 interval of each segment are assigned to 0 (i.e., include CDFDs), the remaining time points are assigned to 1. Finally, 50% CDFDs are intentionally removed from two out of seven PMTSs to simulate the noise of which some PMTSs do not contain CDFD.

(3) *Generate PMTS:* Given $\Theta, \hat{\Theta}, Y$ and Z, the process of generating PMTS is the same as that described in Section 4.1. Specifically, if $Y_{t,k} = 1$ and $Z_t = 1$, $\Theta_p^{(k)}$ is used to generate $\mathcal{X}_{p,t}^{(k)}$ and $\hat{\mathcal{X}}_{p,t}^{(k)}$. On the other hand, if $Y_{t,k} = 1$ and $Z_t = 0$, $\Theta_p^{(k)}$ is used to generate $\mathcal{X}_{p,t}^{(k)}$, and $\hat{\Theta}_p^{(k)}$ is used to generate $\hat{\mathcal{X}}_{p,t}^{(k)}$. After generating all the PMTS data, the uniformly distributed noises between $[-0.5\sigma, 0.5\sigma]$ are added to all observations, where $\sigma \in \mathbb{R}^n$ is the standard deviations of each multivariate time series.

Evaluation Metrics To evaluate and compare the effectiveness of the proposed methods and other baseline methods on PMTS, the predicted Y and Z assignments are compared with the Y and Z assignments used to generate the PMTS. To ensure a fair comparison of the effectiveness of the baseline methods with our method, the number of latent states K in all the methods is fixed to the corresponding K used to generate the datasets, thus ensuring that all methods would be evaluated as a K-class classification problem for Y assignments and a 2-class classification problem for Z assignments. Therefore, the macro F-1 scores for the Y assignments are computed for all the methods, where the macro F-1 score is defined as the average of the K F-1 scores where each is the harmonic mean of the precision and recall for predicting each class of Y assignment. The Z assignments are evaluated using F-1 scores: the closer the (macro) F-1 score to 1, the better the result.

Comparison Methods: To the best of our knowledge, as yet there is no integrated method capable of mining CDFD for PMTS generated from controlled experiments. The baseline methods therefore require a two-step procedure to decide the Y assignments and Z assignments separately. For Step-1 to determine the Y assignments, two methods are considered: GMM [Banfield and Raftery 1993] and the state-of-the-art TICC [Hallac et al. 2017b] introduced in Section 2. For Step-2 to determine the Z assignments, this can be considered as a 2-group partitioning problem over the subsequence pairs in PMTS. Three distance-based methods and one model-based method are compared with our approach. *(1) Distance-based methods*: for each latent state obtained from Step-1, the distances of all subsequence pairs are computed using three distance measures for multivariate time series, namely the Euclidean distance, the Dynamic Time Warping-Dependent (DTW-D) [Shokoohi-Yekta et al. 2017] and Dynamic Time Warping-Independent (DTW-I) [Shokoohi-Yekta et al. 2017] distances. The computed distances are then sorted in descending order and the pairs with the top-i largest distances are assigned to contain CDFDs (i.e., $Z_t = 0$). The macro F-1 scores are computed for all possible values of i and the maximal marco F-1 scores of the baseline methods are reported in the tables. *(2) model-based methods*: For each latent state obtained from Step-1, the 2-component GMM [Banfield and Raftery 1993] is used to partition all the subsequences in both the control and experimental time series belonging to the same latent state into 2 groups. For each subsequence pair $(X_t, \hat{X}_t)$, if X_t and $\hat{X}_t$ are partitioned into different groups, Z_t is assigned to 0 (i.e., existing CDFD), otherwise, $Z_t = 1$. In other words, the values of Z_t is decided by an XNOR-gate [xno 2018]. *(3) Baselines using ground-truth latent state assignment:* To explore the performance of the distance-based and model-based methods only on the subproblem of contrast pattern detection (i.e., Z assignment), we also evaluate the comparison method by staring with the ground truth latent state assignments.

Parameters Settings: In effectiveness evaluation, $\lambda = 0.5$, $\beta = 1$, $\gamma = 3$ are used for our methods. For TICC method, the parameters are intensively tuned to achieve the best performance. To a fair evaluation of the effectiveness, the values of K and w are set to the same as those used to generate the synthetic data for all methods.

6.1.2 Performance on Synthetic Datasets: In this subsection, the effectiveness of the baseline methods and the proposed CMP and GCMP are evaluated and the scalability and the parameter sensitivities of the proposed approaches are tested.

Table 2. Effectiveness Performance

(a) macro F-1 scores and running time in seconds of latent state assignments Y on one PMTS

Individual Datasets	Dataset 1		Dataset 2		Dataset 3		Dataset 4	
Method	F-1,	time	F-1,	time	F-1,	time	F-1,	time
TICC	0.519,	3.83s	0.375,	7.61s	0.284,	13.13s	0.355,	9.80s
GMM	0.954,	0.02s	0.798,	0.08s	0.596,	0.12s	0.766,	0.07s
CMP (ours)	**0.992**,	5.54s	**0.940**,	12.83s	**0.889**,	22.81s	**0.885**,	12.25s

(b) macro F-1 scores and running time in seconds of latent state assignment Y on multiple PMTSs

Group Datasets	Dataset 5		Dataset 6		Dataset 7		Dataset 8	
Method	F-1,	time	F-1,	time	F-1,	time	F-1,	time
TICC	0.945,	1.61s	0.560,	21.35s	0.366,	29.91s	0.531,	22.32s
GMM	0.989,	0.02s	0.943,	0.04s	0.876,	0.10s	0.956,	0.06s
GCMP (ours)	**0.989**,	6.47s	**0.995**,	12.83s	**0.995**,	19.55s	**0.996**,	15.12s

(c) F-1 scores and running time in seconds of contrast pattern indicator Z on one PMTS

Individual Datasets	Dataset 1		Dataset 2		Dataset 3		Dataset 4	
Method	F-1,	time	F-1,	time	F-1,	time	F-1,	time
GMM+DTW-I	0.391,	6.78s	0.410,	11.73s	0.402,	19.84s	0.386,	21.33s
GMM+Euclidean	0.434,	0.43s	0.436,	1.33s	0.44,	2.24s	0.393,	3.29s
GMM+DTW-D	0.392,	2.59s	0.415,	4.69s	0.390,	8.60s	0.393,	10.05s
TICC+Euclidean	0.491,	5.43s	0.476,	10.50s	0.475,	19.64s	0.497,	18.54s
TICC+DTW-D	0.465,	6.51s	0.470,	12.28s	0.468,	22.51s	0.498,	20.92s
TICC+GMM-XNOR	0.490,	3.89s	0.444,	7.73s	0.461,	13.29s	0.371,	9.93s
TICC+DTW-I	0.451,	10.73s	0.471,	19.33s	0.474,	33.74s	0.437,	32.27s
GMM+GMM-XNOR	0.765,	0.11s	0.706,	0.22s	0.603,	0.31s	0.591,	0.27s
Euclidean	0.462,	1.51s	0.502,	2.74s	0.515,	4.88s	0.477,	6.55s
DTW-D	0.421,	2.56s	0.469,	4.46s	0.484,	7.68s	0.481,	9.34s
DTW-I	0.421,	6.68s	0.479,	11.37s	0.482,	18.81s	0.477,	20.29s
GMM-XOR	0.810,	0.08s	0.799,	0.14s	0.824,	0.19s	0.778,	0.21s
CMP (ours)	**0.869**,	5.54s	**0.882**,	10.95s	**0.886**,	22.81s	**0.843**,	12.25s

(d) F-1 scores and running time in seconds of contrast pattern indicator Z on multiple PMTSs

Group Datasets	Dataset 5		Dataset 6		Dataset 7		Dataset 8	
Method	F-1,	time	F-1,	time	F-1,	time	F-1,	time
GMM-Euclidean	0.478,	0.47s	0.416,	1.24s	0.391,	5.03s	0.388,	4.95s
GMM-DTW-D	0.472,	0.99s	0.416,	2.18s	0.393,	7.31s	0.402,	7.42s
GMM-DTW-I	0.454,	2.43s	0.411,	6.63s	0.415,	17.32s	0.423,	13.12s
TICC-Euclidean	0.388,	2.15s	0.471,	24.86s	0.543,	39.51s	0.433,	29.77s
TICC-DTW-D	0.388,	2.61s	0.481,	25.99s	0.550,	42.14s	0.440,	31.74s
TICC-DTW-I	0.386,	4.40s	0.473,	30.35s	0.555,	51.76s	0.453,	41.05s
TICC-GMM-XNOR	0.495,	1.90s	0.388,	23.42s	0.419,	34.62s	0.320,	25.00s
GMM-GMM-XNOR	0.469,	0.08s	0.279,	0.13s	0.350,	0.29s	0.342,	0.17s
GCMP (ours)	**0.842**,	6.82s	**0.976**,	14.38s	**0.866**,	23.77s	**0.975**,	17.31s

Effectiveness Evaluation:

The results of the effectiveness evaluation on Y assignments, are shown in Table 2(a) and Table 2(b) for the individual and group datasets, respectively. Table 2(c) and Table 2(d) list the effectiveness evaluation results for Z assignments,

where the two-step comparison methods with "+" show the results of Z assignments based on the Y assignments predicted by the first step, and the comparison methods without "+" sign show the results of Z assignments based on the ground truth latent state assignments.

As the results shown, our integrated methods outperform the comparison methods for both the Y and Z assignments, while none of other methods perform well on the Z assignments since they are unable to capture the dependency between the latent states and the CDFD patterns. As shown in Table 2a and 2b, the macro F-1 scores of our models on Y (i.e., latent state) assignments achieve the highest macro F-1 scores of 0.960 on average, while the best comparison method can only achieve 0.860. These results are impressive considering the data are noisy, and are generated by the Toeplitz inverse covariance matrix that is not assumed by our models. In contrast, TICC only achieves macro F-1 score at most 0.52 even after we intensively tuned its parameters. GMM runs very fast but performs worse than our models due to the absence of the temporal and the structural regularization terms. Notice that the running time of our algorithm, as an integrated method, is not only for Y assignments but also for Z assignments.

The results on Z assignments for one PMTS are shown in Table 2c and 2d. Our methods achieve the average F-1 score of 0.896, while the best two-step methods only achieve the average F-1 score of 0.513. Even starting with the ground truth Y assignments, the best comparison method only achieves the average F-1 score of 0.803, which is still 10% worse than our methods. The distance based methods are all close to random guess since they are unable to mine the dependency patterns.

In addition, the results for the group datasets validate that our GCMP model is robust enough to capture the CDFDs in noisy data. Furthermore, when the datasets include multiple PMTSs, our GCMP model performs even better than the CMP model. Because by adding an $L_{2,1}$-norm regularization term to the probabilistic model, the GCMP model is able to take all the PMTSs data into account while maintaining the dependency pattern among all the MRFs. It is very important to utilize all the available data in controlled experiments that typically require the data generated by a group of participants.

Scalability Analysis: One iteration of our E-M style algorithm consists of optimizing the Y and Z assignments in the E-step whose complexity is $O(KT)$ as described in the previous section, and optimizing Θ and $\hat{\Theta}$ in the M-step of whose complexity is $O(T)$ for computing the empirical covariances plus $O((nw)^2)$ for our ADMM algorithm. Typically, our ADMM algorithm will give a good enough solution [Boyd et al. 2011] after a few tens of iterations, so the number of iterations in our ADMM algorithm is considered as a constant number. Moreover, T can be potentially in millions which is much larger than K and nw. The total number of iterations of our E-M algorithm depends on the data, but typically converges in dozens of iterations thus can also be considered as a constant number. Therefore, the overall complexity of our algorithm can be considered as $O(T)$ in practice. To validate the scalability of the proposed algorithm, we vary T and compute the running time over one E-M iteration A large dataset is generated by using n=10, w=3, K=10, and $T_{\max}$=10^6. The per-iteration running time, which contains both the E-step and M-step, is plotted using a log-log scale in Figure 4. Our algorithm grows almost linearly over T, and is able to optimize the PMTS with two million data points in about 100 seconds per-iteration using a single thread.

Sensitivity Tests: The sensitivities of the hyper-parameters such as w, λ, β, and γ are tested separately by using a basic setting of $K = 4$, $\lambda = 10$, $\beta = 1$, $\gamma = 3$, $w = 5$ and varying a single parameter each time. The individual and group datasets used here are all generated by the same sequence, namely Datasets 3 and 7. The results of the sensitivity test are plotted in Figure 5. As the Figure 5 shows, both our CMP and GCMP models are relatively insensitive to all the parameters within the range shown. The sensitivities for window sizes w ranging from 2 to 12 are plotted in Figure
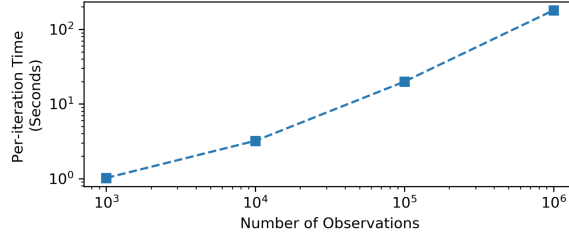
Fig. 4. Per-iteration running time of our algorithm (both E-step and M-step) using a single thread Python program. Our proposed algorithm scales linearly with the number of time points.
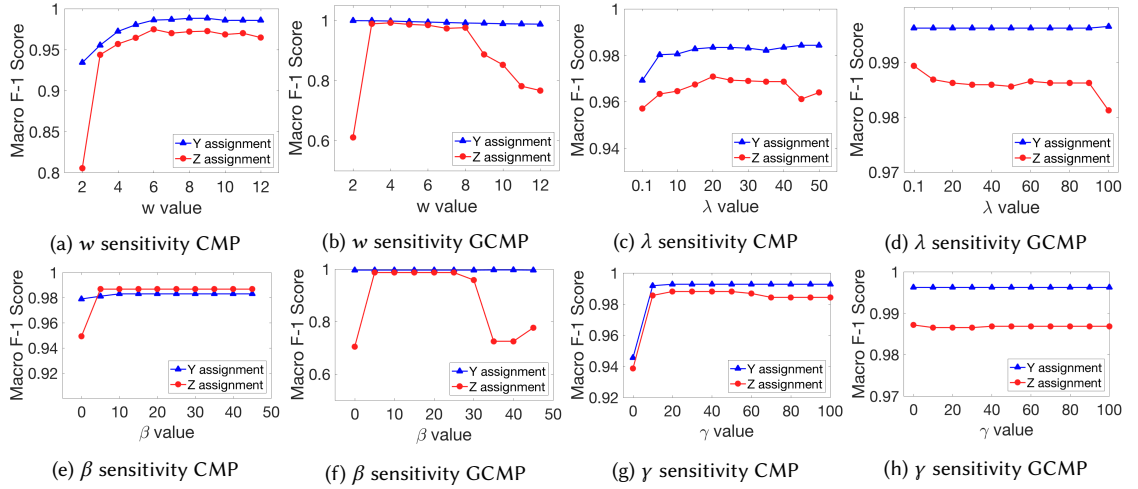

(a) w sensitivity CMP   (b) w sensitivity GCMP   (c) λ sensitivity CMP   (d) λ sensitivity GCMP

(e) β sensitivity CMP   (f) β sensitivity GCMP   (g) γ sensitivity CMP   (h) γ sensitivity GCMP

Fig. 5. Sensitivity Tests

5a and 5b for the individual and group datasets, respectively. Recall the "true" window size of the datasets is 5, so when $w = 2$ the macro F-1 scores are relatively low since neither the models take long term dependencies into account. When $w > 8$, the performance starts to decrease since the model seeks to estimate long term dependencies that are not existing in the datasets. The sensitivity for the three regularization parameters are plotted in Figure 5c to Figure 5h, which demonstrate that any values between 0.1 to 50 work well on the proposed models.

6.2 Experiments on Real-world Datasets

To demonstrate the utility of the CDFD pattern mining task, the proposed CMP and GCMP are applied to a study of contrast driving behaviors by participants diagnosed with ADHD before and after taking their ADHD medication.

6.2.1 Experiment Setup:

Thirteen real-world datasets are obtained by monitoring thirteen ADHD (Attention Deficit Hyperactivity Disorder, a disease that influences human's driving behaviors) participants whose driving behaviors are recorded by a high-fidelity driving simulator. Each dataset contains a pair of multivariate time series of driving data under identical traffic scenarios collected before and after the participants had taken their ADHD medication after a few weeks so that they are unlikely

Manuscript submitted to ACM

to memorize the previous scenarios. Because adding this requirement can prevent the influence on the driving behaviors caused by the memorization, which is an unrelated factor of the controlled experiment. The other detailed protocols of this controlled experiment are described in [Lee et al. 2018].

Translating to PMTS: Even though all the multivariate time series are generated under the same scenarios, due to the various velocities, these time series do not not perfectly match each other along the time-axis. However, the spatial trajectories recorded by their coordinates are very similar, so instead of using time stamp values for the X-axis of these PMTS, we used locations ordered by time to bind the multivariate time series to form the PMTSs defined in Section 3. These PMTSs are therefore translated from the original multivariate time series using the same trajectory to bind all time series. Specifically, all the PMTSs are dynamically rescaled along X-axis from equal time intervals to equal distance intervals in two steps: 1) Randomly selecting one trajectory, then translating it to a *Step-Invariant Trajectory (SIT)* [Li et al. 2017] to serve as the template trajectory such that the distances between any consecutive points are equal to the step distance parameter δ. Here, we set $\delta = 1$ foot. 2) For each spatial point in the template trajectory, the corresponding values of the other sensors are then estimated by linear interpolation to obtain a PMTS dataset whose multivariate time series are all indexed by the same sequence of locations ordered by time.

6.2.2 Performance of CMP. To validate the effectiveness of CMP, the model is applied to an individual dataset with one PMTS. For any value of $K \geq 4$, the model assigns most of the points to four latent states, so let K=4 for this dataset. Each of the resulting latent states can be naturally interpreted as a unique driving state that can be validated by observing the trajectory and the PMTS in Figure 6. For example, the latent state plotted in red in PMTS View can be interpreted as slowing down since the values of the red segments are high in the brake dimension and decrease in the velocity dimension; the orange latent state can be interpreted as turning since all the orange segments correspond to corners, as highlighted in Trajectory View; the green latent state can be interpreted as driving in a straight line since the values of green segments are high in the gas pedal dimension and close to 0 in the steering dimension and the blue latent state can be interpreted as the switching lanes since the values of the blue segments are high in the steering dimension, then change rapidly to the other direction.

To locate the CDFD, the segments containing CDFD (i.e., Z_t=0) are shaded. Recall that the edge in an MRF represents a *Partial Correlation* [Rue and Held 2005] between two connected features. The Partial Correlation (PC) between feature F_1 and feature F_2, denoted as $\boldsymbol{pc}(F_1, F_2)$, measures their "true" correlation which excludes the effect of the other features. We thus visualize the MRFs by plotting their PC networks. Due to the limited space, only the PC networks corresponding to "turning" are plotted in MRF view in Figure 6. Each node in the PC network represents a feature and each solid/dashed edge represents a positive/negative PC. Naturally, the CDFD patterns can be visualized by plotting the differences between $\boldsymbol{pc}(\cdot, \cdot)$ (i.e., before medication) and $\widehat{\boldsymbol{pc}}(\cdot, \cdot)$ (i.e., after medication) in the residual PC View in Figure 6 whose weight of the edge between F_1 and F_2 is defined as: $\boldsymbol{r}(F_1, F_2)$=$\widehat{\boldsymbol{pc}}(F_1, F_2)$−$\boldsymbol{pc}(F_1, F_2)$. All negative/positive weights in the residual PC network are plotted in blue/red, respectively.

The CDFD can be interpreted as the different driving behaviors collected before and after medication. For example, after medication, $\boldsymbol{r}(B_t, B_{t+1})$, $\boldsymbol{r}(G_t, G_{t+1})$ and $\boldsymbol{r}(V_t, V_{t+1})$ are all positive while turning which means that these sensors at index t are more correlated to themselves at the next index after medication. It could be interpreted as this ADHD driver controlling the gas and brake pedals more smoothly after taking her/his medication. While $\boldsymbol{r}(S_t, S_{t+1}) < 0$ suggests the steering wheel is less correlated to the steering wheel at the next index, indicating that, after taking medication, the ADHD participant is more likely to adjust the steering wheel proactively. In addition, $\boldsymbol{r}(V_t, S_t)$ and
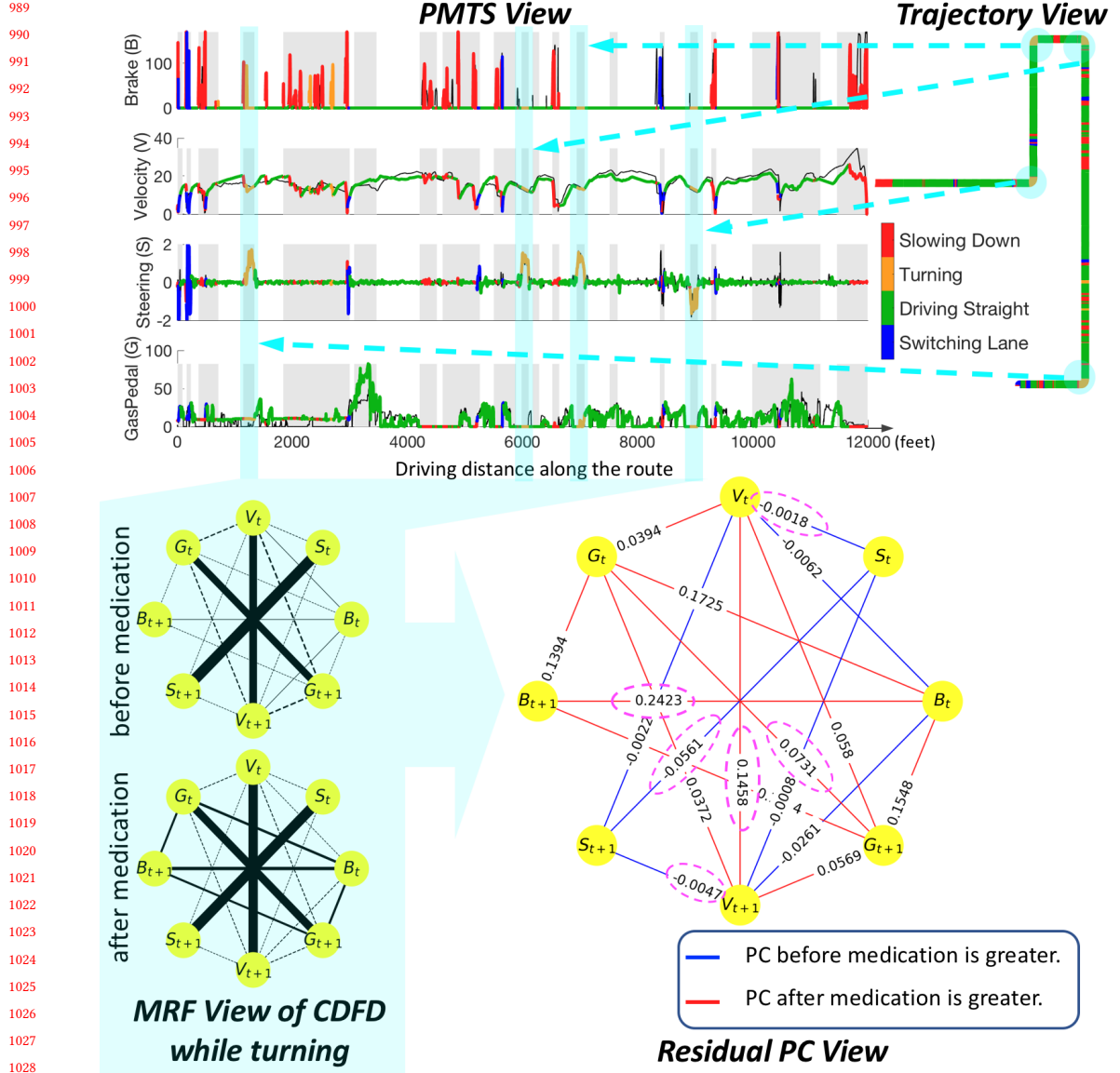
Fig. 6. The contrast patterns, which show some of the driving behaviors changed by the ADHD medication, are plotted in four views. Each latent state is plotted using a unique color in both Trajectory and PMTS View. In PMTS view, the multivariate time series plotted in four colors recorded the driving behaviors after medication. Since the two multivariate time series in PMTS share the same latent state assignments, the multivariate time series before medication is plotted in black. The road segments with contrast patterns are shaded in grey (i.e., Z_t=0) and/or highlighted in cyan (*i.e.*, $Y_{t,\text{Turning}}$=1 and Z_t=0). The partial correlation (PC) networks of latent state "turning" are plotted in MRF view, and the differences of the PC networks are plotted in residual PC view.

$r(V_{t+1}, S_{t+1})$ are both negative, which indicates the velocity is less correlated with the steering wheel, indicating safe handling of steering wheel, when the velocity is high.

Manuscript submitted to ACM

To conclude, the CDFDs showed that before medication, this ADHD participant is more likely to turn the vehicle primarily by adjusting the gas and brake pedals. In contrast, after medication, the same participant is more likely to turn the vehicle by proactively adjusting the steering wheel based on current velocity and adjusting the gas and brake pedals more smoothly.

6.2.3 Performance of GCMP: To validate the effectiveness of GCMP, the model is then applied to the group dataset with all thirteen PMTSs. The experimental settings are the same as those described Section 6.2.1. As shown in Figure 7, the results of the Y assignments and the interpretations are very similar to those seen previously since all participants drove under identical traffic scenarios so the drivers are mostly under the same driving state at the same location. To validate and interpret the CDFD, which contains thirteen pairs of MRFs, a paired T-test is performed and plotted in the T-test *PC* view of Figure 7. The edges in the network denote the existence of significant differences (i.e., the p-value is less than 0.05) between the corresponding PCs before and after medication. Similarly to residual *PC* network seen previously, the edges in the T-test network are plotted in red if the PCs increased significantly after medication (i.e., a positive T-statistic), otherwise, the edges are plotted in blue.

The driving state for line switching is then analyzed. Our model suggested some segments that are circled in the trajectory view of Figure 7 do not contain CDFD, and others, which are highlighted in the PMTS and trajectory views contain CDFD patterns. After examining the original videos, the switching lane state actually contained two cases: passing a slow vehicle and avoiding a sudden cut-in vehicle. The segments marked as no CDFD (i.e., $Z_t = 0$) mostly correspond to the former cases, and the CDFD segments correspond to the latter cases. This indicates that the drivers mostly drive in a similar way when they are switching lanes to pass a slow vehicle in both medication conditions, but switch lanes in different ways before and after medication when another vehicle suddenly cut into their current lane. In this case, the $\widehat{PC}(B_t, B_{t+1})$ are significantly (i.e., the p-value is 0.018) less than $PC(B_t, B_{t+1})$, signifying a stronger reaction (i.e., a weaker PC) on the brake pedals when the ADHD participants switch lanes to avoid crashing into the cut-in vehicles after medication, consequently the $\widehat{PC}(V_t, V_{t+1})$ are also significantly (i.e., the p-value is 0.00096) less than $PC(V_t, V_{t+1})$. Even though all the participants successfully avoid crashes with the cut-in vehicles in both medication conditions, their ways of avoiding the cut-in vehicles are quite different between the before and after medication conditions. As the T-test *PC* view of Figure 7 illustrates, $\widehat{PC}(V_t, S_t)$ is significantly less than $PC(V_t, S_t)$ which means these ADHD participants are more capable of stabilizing their vehicles when avoiding the crash with the cut-in vehicles after medication.

In conclusion, the CDFDs show that after medication the ADHD participants react by braking strongly to slow down and stabilize their vehicles when interacting with cut-in vehicles, thus demonstrating better driving behaviors.

6.3 Additional results on real-world datasets

The contrast patterns for 4 out of 13 ADHD participants, namely Driver A to Driver D, are plotted in Figure 8 to Figure 10. As seen in these figures, while each PMTS is fed to our CMP model independently, the latent state assignments (i.e., Y assignments) and their interpretations are almost the same for all drivers, which validated the effectiveness of our CMP model again. However, their contrast patterns are quite different which can be potentially used to quantify the effects of the ADHD medication on each ADHD driver's driving behavior. The effects of the ADHD medication can be quantified by our model in two aspects:

(1) $e = \frac{\text{count}(\{t|Z_t=0\})}{T} \times 100\%$, which is the percentage of the road segments with contrast patterns, (i.e., the shaded parts plotted in Figure 8 to Figure 10 that indicates the ADHD medication takes effect on the ADHD driver's
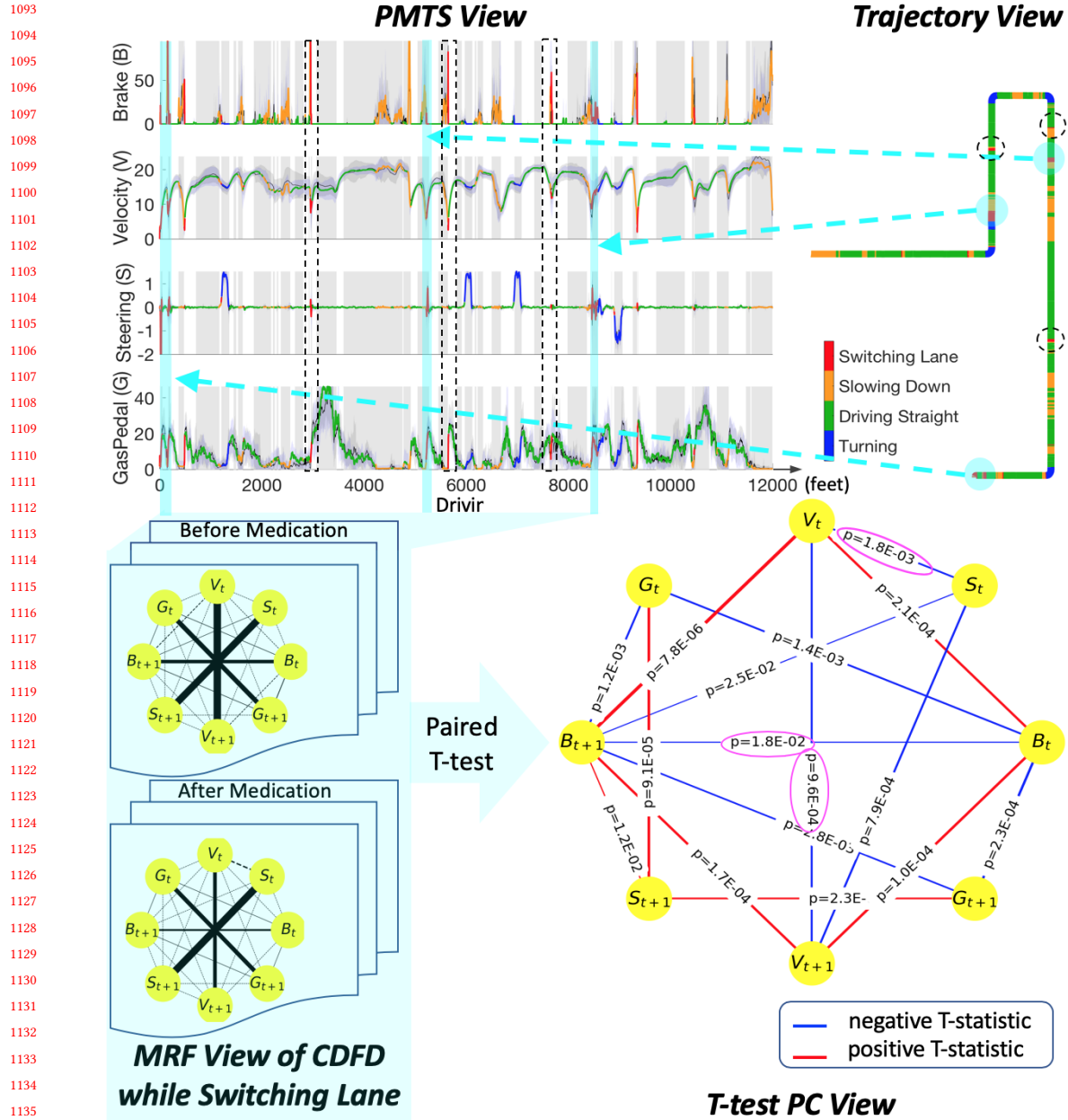
Fig. 7. The group contrast patterns, which show some of the driving behaviors of thirteen participants are changed by the ADHD medication. The views are similar to Figure 6 except for: 1). the mean and standard deviation of the thirteen PMTSs are plotted in PMTS view, 2) thirteen pairs of partial correlation (PC) networks in switching lane latent state are plotted in MRF view, 3) paired T-test is performed on these PC networks in T-test PC view.
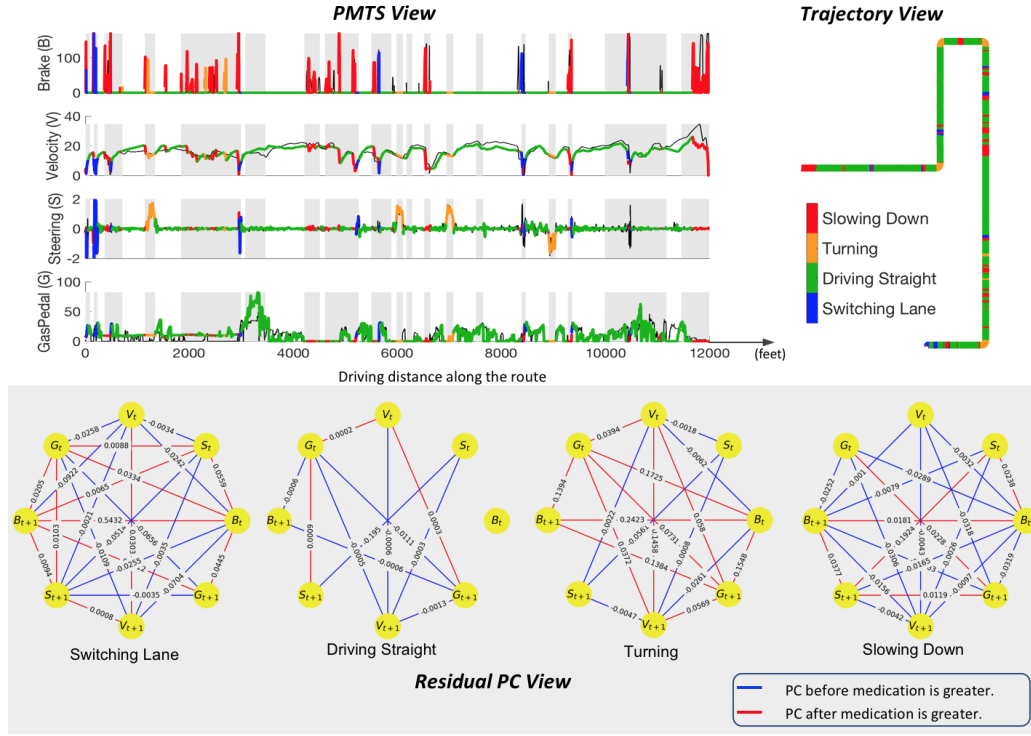
Fig. 8. *Driver A*

Driver	A	B	C	D
e	53.2%	83.4	46.9%	38.7%

Table 3. Percentages of road segments with contrast patterns

driving behaviors). Different patients have different sensitiveness to the medication, the higher value of e, the more sensitive of the ADHD medication to the ADHD driver. The results are shown in Table 3. For example, our model suggests Driver B (i.e., $e_B = 83.4\%$) is more sensitive to the ADHD medication than driver D (i.e., $e_D = 38.7)\%$.

(2) $r(\cdot, \cdot) = \hat{pc}(\cdot, \cdot) - pc(\cdot, \cdot)$, which quantifies how much difference between the driving behaviors before and after medication by the difference of the corresponding partial correlations. As seen in Figure 8 - Figure 10, the ADHD medication changes the driving behaviors of different ADHD drivers in different ways, that is, after medication, some PCs remain the same while other PCs increase or decreases. More importantly, it is only meaningful to quantify the changes by summarizing all the subsequences under the same latent state for controlled experiments, which prohibited the traditional methods applied to the contrast pattern mining problem.
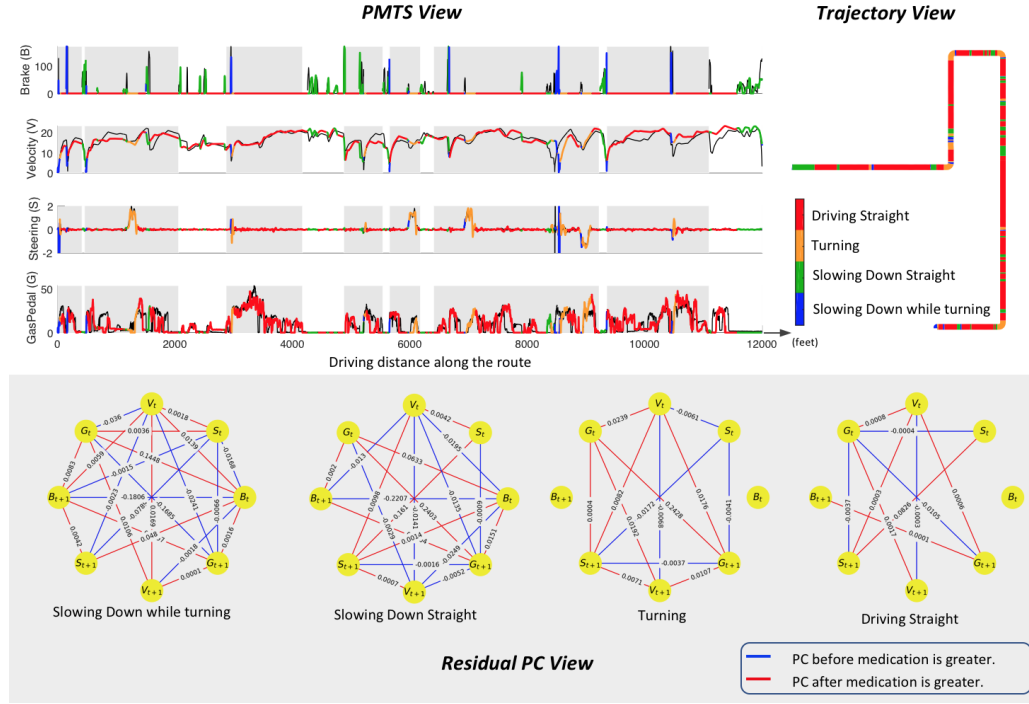
Fig. 9. *Driver B*

7 CONCLUSION

In this paper, we proposed a novel framework to mine interpretable CDFD for PMTS in controlled experiments. In this framework, the CDFD pattern mining problem is formulated as an optimization problem which integrates latent state identification, paired dependency networks inference and contrast pattern detection. To model the optimization problem, we proposed a new probabilistic group graphical lasso which forces the identical structure constraint in paired inverse covariance matrices by adding an $L_{2,1}$-norm regularization term. An efficient algorithm based on E-M and ADMM frameworks is also proposed to solve the graphical lasso. Extensive experimental evaluations on synthetic datasets demonstrated the effectiveness, scalability and robustness of the proposed approach. Additional experiments on real-world datasets demonstrate the utility and interpretability on the mined CDFDs patterns.

REFERENCES

2018. http://www.electronics-tutorial.net/digital-logic-gates/xnor-gate/index.html

Maya Abou-Zeid, Isam Kaysi, and Hani Al-Naghi. 2011. Measuring aggressive driving behavior using a driving simulator: an exploratory study. In *3rd International Conference on Road Safety and Simulation*.

Anurag A Agrawal and Peter M Kotanen. 2003. Herbivores and the success of exotic plants: a phylogenetically controlled experiment. *Ecology Letters* 6, 8 (2003), 712–715.

Jeffrey D. Banfield and Adrian E. Raftery. 1993. Model-Based Gaussian and Non-Gaussian Clustering. *Biometrics* 49, 3 (1993), 803–821. http://www.jstor.org/stable/2532201

Stephen Boyd, Neal Parikh, Eric Chu, Borja Peleato, and Jonathan Eckstein. 2011. Distributed Optimization and Statistical Learning via the Alternating Direction Method of Multipliers. *Foundations and Trends in Machine Learning* 3, 1 (2011), 1–122. https://doi.org/10.1561/2200000016

A. P. Dempster, N. M. Laird, and D. B. Rubin. 1977. Maximum likelihood from incomplete data via the EM algorithm. *JOURNAL OF THE ROYAL STATISTICAL SOCIETY, SERIES B* 39, 1 (1977), 1–38.
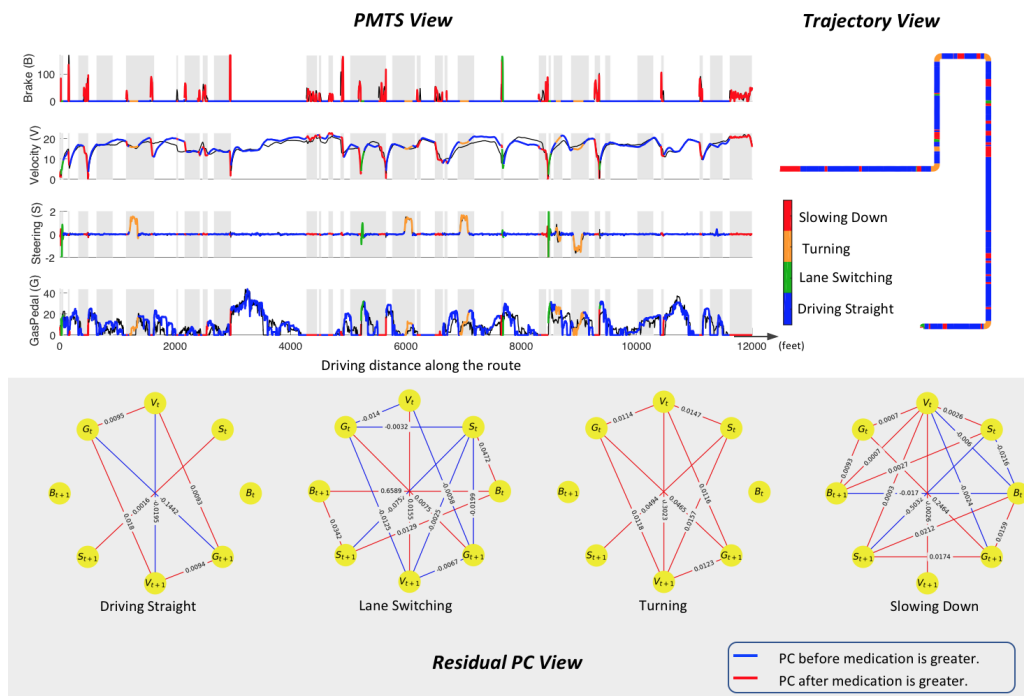
Fig. 10. *Driver C*

D. Donoho, I. Johnstone, and Iain M. Johnstone. 1993. Ideal Spatial Adaptation by Wavelet Shrinkage. *Biometrika* 81 (1993), 425–455.

László Erdős, Antti Knowles, Yau, et al. 2013. Spectral statistics of Erdős–Rényi graphs I: local semicircle law. *The Annals of Probability* 41, 3B (2013), 2279–2375.

Jerome Friedman, Trevor Hastie, and Robert Tibshirani. 2008. Sparse inverse covariance estimation with the graphical lasso. *Biostatistics* 9, 3 (2008), 432–441.

Dina Goldin, Ricardo Mardales, and George Nagy. 2006. In search of meaning for time series subsequence clustering: matching algorithms based on a new distance measure. In *Proceedings of the 15th ACM international conference on Information and knowledge management (CIKM '06)*. ACM, 347–356.

David Hallac, Youngsuk Park, Stephen Boyd, and Jure Leskovec. 2017a. Network Inference via the Time-Varying Graphical Lasso. In *Proceedings of the 23rd ACM SIGKDD International Conference on Knowledge Discovery and Data Mining (KDD '17)*. New York, NY, USA, 205–213. https://doi.org/10.1145/3097983.3098037

David Hallac, Sagar Vare, Stephen Boyd, and Jure Leskovec. 2017b. Toeplitz Inverse Covariance-Based Clustering of Multivariate Time Series Data. In *Proceedings of the 23rd ACM SIGKDD International Conference on Knowledge Discovery and Data Mining (KDD '17)*. New York, NY, USA, 215–223. https://doi.org/10.1145/3097983.3098060

Alexander Jung, Gabor Hannak, and Norbert Goertz. 2015. Graphical lasso based model selection for time series. *IEEE Signal Processing Letters* 22, 10 (2015), 1781–1785.

E. Keogh, J. Lin, and W. Truppel. 2003. Clustering of time series subsequences is meaningless: implications for previous and future research. In *Third IEEE International Conference on Data Mining (ICDM '03)*. 115–122. https://doi.org/10.1109/ICDM.2003.1250910

Ross Kindermann and J Laurie Snell. 1980. *Markov random fields and their applications*. Vol. 1.

John Boaz Lee, Xiangnan Kong, Yihan Bao, and Constance Moore. 2017. Identifying Deep Contrasting Networks from Time Series Data: Application to Brain Network Analysis. In *Proceedings of the 2017 SIAM International Conference on Data Mining (SIAM '17)*. SIAM, 543–551.

Yi-Ching Lee, Chelsea Ward McIntosh, Flaura Winston, Thomas Power, Patty Huang, Santiago Ontañón, and Avelino Gonzalez. 2018. Design of an experimental protocol to examine medication non-adherence among young drivers diagnosed with ADHD: A driving simulator study. *Contemporary clinical trials communications* 11 (2018), 149–155.

Qingzhe Li, Jessica Lin, Liang Zhao, and Huzefa Rangwala. 2017. A Uniform Representation for Trajectory Learning Tasks. In *Proceedings of the 25th ACM SIGSPATIAL International Conference on Advances in Geographic Information Systems (SIGSPATIAL'17)*. New York, NY, USA, Article 80, 4 pages. https://doi.org/10.1145/3139958.3140017
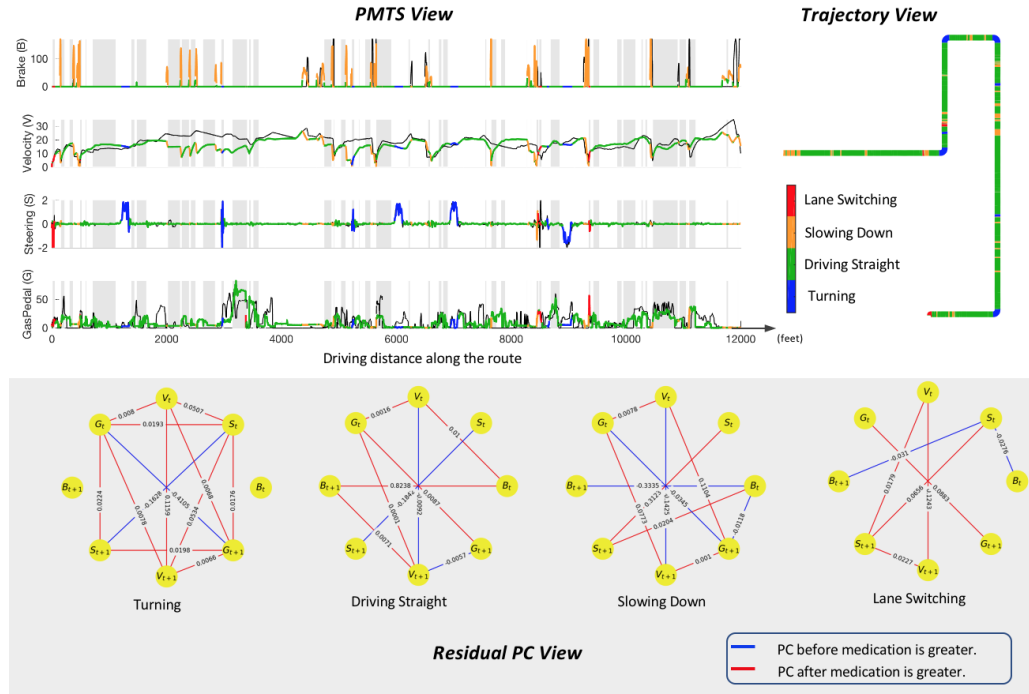
Fig. 11.   *Driver D*

Jessica Lin and Eamonn Keogh. 2006. Group SAX: Extending the Notion of Contrast Sets to Time Series and Multimedia Data. In *Knowledge Discovery in Databases: PKDD 2006 (PKDD '06)*. Berlin, Heidelberg, 284–296.

Xinyue Liu, Xiangnan Kong, and Ann B Ragin. 2017. Unified and Contrasting Graphical Lasso for Brain Network Discovery. In *Proceedings of the 2017 SIAM International Conference on Data Mining (SIAM '17)*. SIAM, 180–188.

Yasuko Matsubara, Yasushi Sakurai, and Christos Faloutsos. 2014. AutoPlait: Automatic Mining of Co-evolving Time Sequences. In *Proceedings of the 2014 ACM SIGMOD International Conference on Management of Data (SIGMOD '14)*. ACM, New York, NY, USA, 193–204.   https://doi.org/10.1145/2588555.2588556

Todd K Moon. 1996. The expectation-maximization algorithm. *IEEE Signal processing magazine* 13, 6 (1996), 47–60.

Thanawin Rakthanmanon, Eamonn J Keogh, Stefano Lonardi, and Scott Evans. 2012. MDL-based time series clustering. *Knowledge and information systems* 33, 2 (2012), 371–399.

Havard Rue and Leonhard Held. 2005. *Gaussian Markov random fields: theory and applications.*

Gideon Schwarz et al. 1978. Estimating the dimension of a model. *The annals of statistics* 6, 2 (1978), 461–464.

Mohammad Shokoohi-Yekta, Bing Hu, Hongxia Jin, Jun Wang, and Eamonn Keogh. 2017. Generalizing DTW to the multi-dimensional case requires an adaptive approach. *Data mining and knowledge discovery* 31, 1 (2017), 1–31.

Padhraic Smyth. 1997. Clustering Sequences with Hidden Markov Models. In *Advances in Neural Information Processing Systems 9*, M. C. Mozer, M. I. Jordan, and T. Petsche (Eds.). 648–654.   http://papers.nips.cc/paper/1217-clustering-sequences-with-hidden-markov-models.pdf

Erica CG van Geffen, Daphne Philbert, Carla van Boheemen, et al. 2011. Patients' satisfaction with information and experiences with counseling on cardiovascular medication received at the pharmacy. *Patient education and counseling* 83, 3 (2011), 303–309.

Vivek Veeriah, Rohit Durvasula, and Guo-Jun Qi. 2015. Deep Learning Architecture with Dynamically Programmed Layers for Brain Connectome Prediction. In *Proceedings of the 21th ACM SIGKDD International Conference on Knowledge Discovery and Data Mining (KDD '15)*. New York, NY, USA, 1205–1214.   https://doi.org/10.1145/2783258.2783399

Andrew Viterbi. 1967. Error bounds for convolutional codes and an asymptotically optimum decoding algorithm. *IEEE transactions on Information Theory* 13, 2 (1967), 260–269.

Xing Wang, Jessica Lin, Pavel Senin, Tim Oates, Sunil Gandhi, Arnold P. Boedihardjo, Crystal Chen, and Susan Frankenstein. 2016. RPM: Representative Pattern Mining for Efficient Time Series Classification. In *EDBT (EDBT '16)*.

Yimin Xiong and Dit-Yan Yeung. 2004. Time series clustering with ARMA mixtures. *Pattern Recognition* 37, 8 (2004), 1675 – 1689. https://doi.org/10.1016/j.patcog.2003.12.018

Lexiang Ye and Eamonn Keogh. 2009. Time Series Shapelets: A New Primitive for Data Mining. In *Proceedings of the 15th ACM SIGKDD International Conference on Knowledge Discovery and Data Mining (KDD '09)*. New York, NY, USA, 947–956. https://doi.org/10.1145/1557019.1557122

TP Yuen, H Wong, and KFC Yiu. 2018. On constrained estimation of graphical time series models. *Computational Statistics & Data Analysis* (2018).